Published online 16 February 2023

Nucleic Acids Research, 2023, Vol. 51, No. 5 ***2195–2214***
https://doi.org/10.1093/nar/gkad057

p38-mediated FOXN3 phosphorylation modulates lung inflammation and injury through the NF-κB signaling pathway

Xinxing Zhu[1,*,†], Beijia Huang[1,†], Fengting Zhao[1], Jie Lian[1,2], Lixiang He[3], Yangxia Zhang[1], Longkai Ji[1], Jinghang Zhang[3], Xin Yan[4], Taoling Zeng[5], Chunya Ma[1], Yinming Liang[6], Chen Zhang[7] and Juntang Lin[1,2,*]

[1]Henan Joint International Research Laboratory of Stem Cell Medicine, School of Medical Engineering, Xinxiang Medical University, Xinxiang 453003, China, [2]Stem Cells and Biotherapy Engineering Research Center of Henan, National Joint Engineering Laboratory of Stem Cells and Biotherapy, School of Life Science and Technology, Xinxiang Medical University, Xinxiang 453003, China, [3]Department of Pathology, The First Affiliated Hospital of Xinxiang Medical University, Xinxiang 453003, China, [4]Translational Neurodegeneration Section Albrecht-Kossel, Department of Neurology, University Medical Center Rostock, Rostock 18147, Germany, [5]State Key Laboratory ofCellular Stress Biology, Innovation Center for Cell Biology, School of LifeSciences, Xiamen University, Fujian 361102, China, [6]Laboratory of Genetic Regulators in the Immune System, Henan Collaborative Innovation Center of Molecular Diagnosis and Laboratory Medicine, School of Laboratory Medicine, Xinxiang Medical University, Xinxiang 453003, China and [7]Department of Neurobiology, School of Basic Medical Sciences, Beijing Key Laboratory of Neural Regeneration and Repair, Advanced Innovation Center for Human Brain Protection, Capital Medical University, Beijing 100069, China

Received August 11, 2022; Revised December 23, 2022; Editorial Decision January 14, 2023; Accepted January 19, 2023

ABSTRACT

NF-κB activates the primary inflammatory response pathway responsible for methicillin-resistant *Staphylococcus aureus* (MRSA)-induced lung inflammation and injury. Here, we report that the Forkhead box transcription factor FOXN3 ameliorates MRSA-induced pulmonary inflammatory injury by inactivating NF-κB signaling. FOXN3 competes with IκBα for binding to heterogeneous ribonucleoprotein-U (hnRNPU), thereby blocking β-TrCP-mediated IκBα degradation and leading to NF-κB inactivation. FOXN3 is directly phosphorylated by p38 at S83 and S85 residues, which induces its dissociation from hnRNPU, thus promoting NF-κB activation. After dissociation, the phosphorylated FOXN3 becomes unstable and undergoes proteasomal degradation. Additionally, hnRNPU is essential for p38-mediated FOXN3 phosphorylation and subsequent phosphorylation-dependent degradation. Functionally, genetic ablation of FOXN3 phosphorylation results in strong resistance to MRSA-induced pulmonary inflammatory injury. Importantly, FOXN3 phosphorylation is clinically positively correlated with pulmonary inflammatory disorders. This study uncovers a previously unknown regulatory mechanism underpinning the indispensable role of FOXN3 phosphorylation in the inflammatory response to pulmonary infection.

GRAPHICAL ABSTRACT

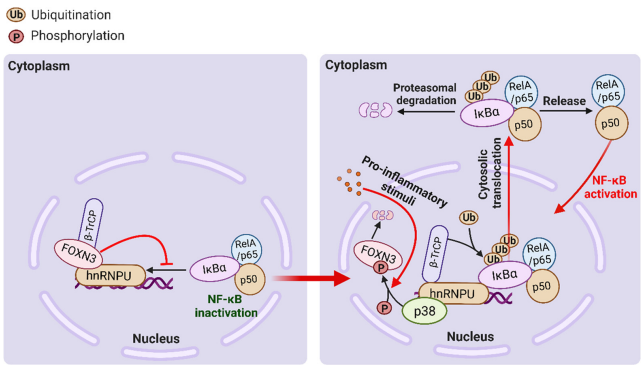

*To whom correspondence should be addressed. Email: linjtlin@126.com
Correspondence may also be addressed to Xinxing Zhu. Email: zhuxinxing0202@163.com
†The authors wish it to be known that, in their opinion, the first two authors should be regarded as Joint First Authors.
Present address: Xinxing Zhu, Henan Joint International Research Laboratory of Stem Cell Medicine, School of Medical Engineering, Xinxiang Medical University, JinSui Road #601, Xinxiang City, Henan Province, China.

INTRODUCTION

As a serious pathogen of humans, *Staphylococcus aureus* (*S. aureus*), and methicillin-resistant *S. aureus* (MRSA) in particular, can trigger numerous, severe and sometimes life-threatening disorders, such as pneumonia and sepsis. The treatment of MRSA-induced diseases has become an extremely complex public health issue due to the widespread antibiotic resistance characteristic of MRSA strains (1–4). MRSA infection in humans frequently leads to acute lung injury, primarily characterized by severe and acute pulmonary inflammation with increased neutrophil influx, alveolar edema triggered by inflammatory neutrophil and macrophage infiltration into the alveolar epithelium, and secretion of numerous inflammatory mediators (5–8). More importantly, an initial acute lung injury from bacterial pneumonia can develop into more severe pulmonary dysfunction, commonly defined as acute respiratory distress syndrome (ARDS). ARDS is one of the most severe pulmonary inflammatory disorders and is associated with high morbidity and mortality in critically ill patients (9–11). Therefore, exploration of new strategies for clinical treatment of MRSA-induced acute lung injury is urgently needed.

Numerous inflammatory signaling pathways participate in MRSA-triggered acute lung injury, among which NF-κB signaling is widely accepted as a central contributing factor. Hence, the modulation of NF-κB activity is essential for improving this pathological process. NF-κB is a key pro-inflammatory transcription factor that is composed of homo- or heterodimers of RelA (p65), RelB, c-Rel, p50/p105 (NF-κB1) or p52/p100 (NF-κB2) (12–15), among which the p65/p50 heterodimer is the major form functionally engaged in the regulation of inflammatory disorders. Interestingly, NF-κB signaling can be mediated by either an IKKβ kinase activity-dependent or -independent mechanism. In the canonical mechanism, cytosolic NF-κB is sequestered via masking of its nuclear localization signal by its main inhibitor IκBα (16,17). In response to proinflammatory stimuli, activated IKKβ can phosphorylate IκBα at its S32 and S36 residues to promote its ubiquitin-mediated degradation by the F-box-containing E3 ligase β-TrCP. IκBα degradation leads to release and nuclear translocation of NF-κB, followed by its transcriptional activation of inflammatory response genes (16,18,19). This regulatory cascade for NF-κB thus depends on IKKβ kinase activity. Recent work has shown that NF-κB signaling can be activated independently of IKKβ kinase activity when subjected to ultraviolet (UV) irradiation (20). In this mechanism, nuclear IKKβ functions as an adaptor protein to facilitate recruitment of heterogeneous ribonucleoprotein-U (hnRNPU), which serves as a bridge to link β-TrCP and IκBα through domain-dependent interactions, consequently resulting in β-TrCP-mediated IκBα degradation and NF-κB activation. There is currently no evidence in the literature supporting whether this nuclear NF-κB could be activated by multiple pro-inflammatory stimuli, although it is well known to be activated by UV irradiation. Hence, it is of great interest to investigate whether this regulatory pattern for NF-κB signaling activation makes any functional contributions to the inflammatory response.

Forkhead box (FOX) proteins belong to a class of transcription factors that share a conserved Forkhead DNA-binding domain, also known as a winged helix domain. There are 19 known subclasses (A to S) of FOX proteins that participate in numerous cellular and physiological processes, including cell proliferation, differentiation, development and tumorigenesis (21–23). Here, in the current study, we defined the transcription factor FOXN3 as a previously unrecognized regulator of IKKβ/hnRNPU-mediated NF-κB activation in the nucleus. FOXN3 overexpression strongly inhibits ubiquitin-mediated IκBα degradation and NF-κB transcriptional activity. Mass spectrometry (MS) analysis revealed a robust association between FOXN3 and hnRNPU, reflecting a potential regulatory role for FOXN3 in modulating NF-κB signaling. In addition, we found that FOXN3 can be directly phosphorylated by p38, and this phosphorylation event contributes to hnRNPU-mediated NF-κB activation. Functionally, genetic disruption of FOXN3 S83 and S85 phosphorylation is strongly resistant to MRSA-induced pulmonary inflammatory injury, indicating the crucial physiological function of FOXN3 S83 and S85 phosphorylation in pulmonary infection-triggered inflammatory injury. In summary, this study identifies a previously unknown regulatory pattern for NF-κB signaling activation and provides a new insight into understanding how NF-κB signaling is activated and functions in response to multiple pro-inflammatory stimuli, especially pulmonary infections.

MATERIALS AND METHODS

Cell culture

Human primary alveolar type II epithelial (ATII) cells were cultured in Dulbecco's modified Eagle's medium/F12 (DMEM/F12). Primary mouse embryonic fibroblasts (MEFs), human bronchial epithelial (BEAS-2B) and HEK293T cells were cultured in DMEM. Culture media were all supplemented with 10% fetal calf serum (Gibco) and 1% penicillin–streptomycin (Millipore) at 37°C in a humidified 5% CO_2 incubator. The human primary ATII cells were obtained from iCell Bioscience (Shanghai, China). BEAS-2B and HEK293T cells were purchased from the American Type Culture Collection (ATCC). MEFs were isolated from mouse embryos at E13.5.

Antibodies and chemical reagents

The following primary antibodies were used: anti-hnRNPU (1:1000, 14599–1-AP, Proteintech), anti-IκBα (1:1000, 10268–1-AP, Proteintech), anti-HA (1:1000, 51064–2-AP, Proteintech), anti-Myc (1:1000, 16286–1-AP, Proteintech), anti-Flag (1:1000, 20543–1-AP, Proteintech), anti-LaminB1 (1:1000, 12987–1-AP, Proteintech), anti-β-actin (1:2000, 66009–1-lg, Proteintech), anti-rabbit IgG (30000–0-AP, Proteintech), anti-p65 (1:200, 10745–1-AP, Proteintech), anti-NF-κB1 (1:200, 14220–1-AP, Proteintech), anti-RelB (1:200, 25027–1-AP, Proteintech), anti-α-tubulin (1:1000, 11224–1-AP, Proteintech), anti-glyceraldehyde phosphate dehydrogenase (GAPDH; 1:1000, 2118, Cell Signaling Technology), anti-IKKβ (1:500, 8943, Cell Signaling Technology), anti-p38 (1:1000,

8690, Cell Signaling Technology), anti-CD68 (1:500, GB11067, Servicebio), anti-FOXN3 (1:500, ab129453, Abcam, for human) and anti-FOXN3 (1:250, A15039, ABclonal, for mouse). Alexa Fluor 555 donkey anti-rabbit (1:500, A31572, Thermo Fisher Scientific) and Alexa Fluor 488 goat anti-rabbit (1:1000, A-11008, Invitrogen) were also used. Phosphospecific antibody against FOXN3 S83/S85 was generated by Dia-An Biotechnology Co, Ltd (Wuhan, China) using the phosphopeptides (VLRSpVSpPVQ) as immunogen. Anti-HA magnetic beads (88836) and anti-DYKDDDDK magnetic beads (A36798) were from Thermo Fisher Scientific. The following chemical reagents were used: lipopolysaccharide (LPS; L6529, Sigma-Aldrich), SB 253080 (HY-10256, MedChemExpress), TBB (HY-14394, MedChemExpress), IMD-0354 (HY-10172, MedChemExpress), MG132 (HY-13259, MedChemExpress), chloroquine (CQ; HY-17589A, MedChemExpress), cycloheximide (CHX; HY-12320, MedChemExpress), leptomycin B (LMB; S1726, Beyotime) and DNase I (M6101, Promega).

Plasmid constructions

Flag-FOXN3, HA-FOXN3, Flag-hnRNPU and HA-hnRNPU were generated by cloning human cDNAs into a pLV-EF1α lentiviral vector. Flag-IκBα, Myc-IκBα, Myc-β-TrCP, HA-p38 and HA-IKKβ were generated by cloning human cDNAs into a pCMV6 vector. Adeno-associated virus (AAV) wild-type (WT) FOXN3 was generated by cloning human FOXN3 cDNAs into a pAAV-CAG adeno-associated viral vector. Point mutations were generated by site-directed mutagenesis. FOXN3 mutants S83A, S85A, S83,85A and S83,85D were produced by using Flag-FOXN3 as the template. Flag-tagged hnRNPU truncated peptides, amino acids 1–238, 238–550 and 550–818, were generated by inserting the respective polymerase chain reaction (PCR)-amplified DNA fragments into a pLV-EF1α lentiviral vector, Flag-hnRNPU was used as the template. Flag-tagged FOXN3 truncated peptides (ΔNTD, ΔForkhead and ΔCTD) and Flag-tagged hnRNPU truncated peptides (Δ1–238, Δ238–550 and Δ550–818) were generated according to the COP-QuickChange (COP-QC) protocol as previously described (24). All constructs generated in this study were verified by DNA sequencing.

Immunoprecipitation and ubiquitination assays

For immunoprecipitation, cells were lysed in a lysis buffer containing 50 mM Tris–HCl (pH 7.4), 150 mM NaCl, 1% Triton X-100 and 1 mM dithiothreitol (DTT), supplemented with a protease and phosphatase inhibitor cocktail. The cell lysates were immunoprecipitated by using appropriate antibodies. The immunoprecipitates were washed four times with the lysis buffer and then subjected to immunoblot analysis. For ubiquitination assay, cells were lysed in a 1% sodium dodecylsulfate (SDS) buffer containing Tris–HCl (pH 7.5), 0.5 mM EDTA and 1 mM DTT. After boiling for 10 min, the cell lysates were diluted 10-fold with Tris–HCl buffer, centrifuged to remove debris and subjected to immunoprecipitation with anti-DYKDDDDK magnetic beads. The immunoprecipitates were boiled and subjected to immunoblot analysis.

Fractionation experiment coupled with DNase I digestion of nuclei or ubiquitination assay

For DNase I digestion of the fractionated nuclei, briefly, 1×10^7 cells were swollen in buffer A [10 mM pH 7.9 HEPES, 1.5 mM $MgCl_2$, 10 mM KCl, 1 mM DTT, 0.5 mM phenylmethylsulfonyl fluoride (PMSF)]. The swollen cells were extracted with buffer A containing 1% NP-40, then subjected to two rounds of extraction with a low-salt buffer A containing 0.5% NP-40 and 75 mM NaCl. The supernatants of three rounds of extraction were combined and saved as the low-salt fraction (LSF). The low-salt-extracted nuclei (LSEN) were incubated with DNase I at 30°C for 1.5 h digestion, followed by centrifugation at 10 000 *g* for 5 min. The supernatant and the digested nuclei were lysed by SDS-loading buffer and subjected to immunoblot analysis. The detailed procedure was performed as previously reported (25). For nucleocytoplasmic fractionation, the cytosolic and nuclear fractions were extracted using a kit (P0027, Beyotime, Beijing) according to the manufacturer's instruction. For nuclear ubiquitination analysis, the cytosolic fraction of cells was extracted and discarded using the nucleocytoplasmic fractionation kit, and the extracted nuclei were lysed in a 1% SDS buffer containing Tris–HCl (pH 7.5), 0.5 mM EDTA and 1 mM DTT. Subsequently, the detailed procedure was performed according to the ubiquitination assay described above.

Lentivirus and adeno-associated virus infection

For AAV infection, the AAV6 system was used for stably overexpressing specific factors in lungs of mice. AAV-based core plasmid expressing indicated factor, together with pAAV-RC6 and pHelper plasmids, were co-transfected into HEK293A cells for the production of AAV. The AAV was extracted using a AAVpro Purification Kit (6666, Takara) according to the manufacturer's instructions 72 h after the transfection. The purified AAV was titrated with an AAVpro titration Kit (6233, Takara). After quantification, the AAV (1×10^{12} vg/ml) was intratracheally instilled into lungs of mice for further studies. For lentivirus infection, the detailed procedures were conducted as previously described (26).

shRNA knockdown

For short hairpin RNA (shRNA) knockdown, the target sequences of shRNAs were cloned into a pHBLV-U6 lentiviral vector, and the production of lentiviral particles was carried out as previously described (26). The sequences of shRNAs used were as follows: shFOXN3, 5′-GCCTGACATCCGATTAGAA-3′; shhnRNPU, 5′-AGATCATGGCCGTGGATATTT-3′; shp38#1, 5′-CCATGAGGCAAGAAACTATAT-3′; and shp38#2, 5′-CCATTTCAGTCCATCATTCAT-3′.

In vitro kinase assay

For the *in vitro* kinase assay, bacterially expressed p38, WT FOXN3 and its mutant S83,85A proteins were incubated in a reaction buffer containing 20 mM Tris–HCl (pH 7.5), 10 mM $MgCl_2$, 1 mM DTT and 25 μM ATP at 37°C for

1 h. After incubation, the phosphorylation levels of WT FOXN3 and its mutants were detected by using a phospho-specific antibody.

Animal studies

Male C57BL/6 mice (aged 8–10 weeks) were used in this study. All animal experiments were approved by the Institutional Review Board of Xinxiang Medical University, and the procedures were performed in accordance with the institutional guidelines of Xinxiang Medical University. The study was compliant with all relevant ethical regulations regarding animal research.

FOXN3 S83,85A knock-in and knockout mice

FOXN3 S83,85A knock-in (KI) and FOXN3 knockout (KO) mice were generated by using the CRISPR/Cas9 [clustered regularly interspaced palindromic repeats (CRISPR)/CRISPR-associated peptide 9] gene editing system. For FOXN3 S83,85A KI mice, the S83 and S85 residues of FOXN3 were both mutated to alanine on the C57BL/6 background. The point mutations were introduced by CRISPR/Cas9-mediated knock-in experiments which involve preparation of single guide RNA (sgRNA), Cas9 mRNA and synthetic single-stranded oligodeoxynucleotide (ssODN) donors prior to microinjection and transplantation of the fertilized eggs as described in previous studies (27,28). The CRISPR/Cas9 sgRNA including the target sequence and the protospacer adjacent motif (PAM; TAGGAGTGTCAGTCCTGTGCAGG) were synthesized by GenScript (Nanjing, China). Genotyping of the mutant mice was performed by Sanger sequencing. For FOXN3-KO mice, gRNA1 (CCGACATCCGATTAGAAGAGGGG) and gRNA2 (ATGGTGGGGTGTCATCGTCTAGG) were used to target the sequence within exon 2 of FOXN3. Genotyping of the mice was performed using PCR with the following primer sequences: forward, 5′-GTAGTTGAGAGCCAGATAGGAGC-3′; reverse, 5′-TCCTCTCTTTGTCCACTTTCTTGA-3′.

Histological assays

For histological analysis, lungs of mice were fixed in 4% paraformaldehyde, embedded in paraffin and sectioned at 4 μm. The sections were then subjected to hematoxylin and eosin (H&E) staining. For immunohistochemical staining, tissue slides were first baked at 60°C for 2 h followed by deparaffinization with xylenes and rehydration through an ethanol gradient. The slides were then subjected to antigen retrieval by heating at 95°C in citrate buffer (10 mM sodium citrate, pH 8.5) for 30 min and cooling down to room temperature. After blocking of endogenous peroxidase activity and serum sealing, the sections were incubated with appropriate primary and secondary antibodies, then subjected to a 3,3′-diaminobenzidine (DAB) chromogenic reaction with DAB color developing solution. After the nucleus counterstaining and dehydration, the tissue slides were visualized and captured by using an inverted microscope.

Immunofluorescence assay

Cells grown on glass coverslips were fixed with 4% paraformaldehyde after washing three times with phosphate-buffered saline (PBS), followed by permeabilization with 0.25% Triton X-100. The cells were then stained with appropriate primary and Alexa Fluor 555- or Alexa Fluor 488-conjugated secondary antibodies. Images were obtained by using a confocal microscope.

Mass spectrometry

The MS analysis was performed on a Q-Exactive mass spectrometer (Thermo Fisher Scientific) equipped with a Nanospray Flex source (Thermo Fisher Scientific). The peptide mixtures were loaded by a capillary C18 trap column (3 cm × 100 μm, C18, 3 μm, 150 Å) and separated by a C18 column (15 cm × 75 μm, C18, 3 μm, 120 Å) on an ChromXP Eksigent system (ABSciex). The flow rate was 300 nl/min and the linear gradient was 70 min (0–0.5 min, 95–92% A; 0.5–48 min, 92–74% A; 48–61 min, 74–62% A; 61–61.1 min, 62–15% A; 61.1–67 min, 15% A; 67–67.1, 15–95% A; 67.1–70 min, 95% A. Mobile phase A = 2% acetonitrile (ACN)/0.1% formic acid (FA) and B = 95% ACN/0.1% FA. Full MS scans were acquired in the mass range of 300–1600 m/z with a mass resolution of 70 000, and the AGC target value was set at 1e6. The 10 most intense peaks in MS were fragmented with higher energy collisional dissociation with a collision energy of 30. MS/MS spectra were obtained with a resolution of 17 500 with an AGC target of 2000 00 and a maximum injection time of 50 ms. The QE dynamic exclusion was set for 15.0 s and run under positive mode. The MS data were processed and analyzed with the help of Oebiotech Co., Ltd (Shanghai, China). The raw data have been deposited to the ProteomeXchange Consortium (http://proteomecentral.proteomexchange.org) via the iProX partner repository with the dataset identifier PXD032864.

Intratracheal administration of AAV or MRSA

MRSA strain 43300 (ATCC) grown to mid-exponential phase at 37°C in Luria–Bertani (LB) medium was centrifuged and resuspended with sterile PBS. For AAV and MRSA administration, ∼50 μl of PBS solution containing 1×10^{12} vg/ml AAV was first intratracheally instilled into lungs of mice, followed by MRSA intratracheal infection (2×10^8 to 5×10^8 colony-forming units per mouse) 3 weeks after AAV administration. The mice were then euthanized 24–48 h after MRSA infection and lung tissues were collected for subsequent analysis.

Bronchial alveolar lavage (BAL) fluid acquisition and analysis

Lungs of mice were lavaged three times with 0.8 ml of ice-cold PBS to collect the BAL fluid. The BAL fluid was centrifuged at 4°C to obtain the cell-free supernatant. This supernatant was directly used to determine the levels of total protein and pro-inflammatory factors, as well as the neutrophil-associated myeloperoxidase (MPO) activity and white blood cell (WBC) counts. The total protein

level was measured by a bicinchoninic acid (BCA) protein assay kit (P0010S) from Beyotime (Shanghai, China), and the pro-inflammatory factors interleukin (IL)-1β and IL-6 were detected by two enzyme-linked immunosorbent assay (ELISA) kits (88–7013-22 and 88–7064-22, Invitrogen). The MPO activity was assessed by an ELISA kit from Abcam (ab155458).

Quantitative real-time PCR analysis

Total RNAs were isolated from cells using Trizol reagent according to the manufacturer's instructions. Reverse transcription was performed with 1 μg of total RNA using a 5× All-In-One RT Kit (G486, Applied Biological Materials). Quantitative real-time PCR was performed using an EvaGreen qPCR Master Mix (G891, Applied Biological Materials). The relative changes of gene expression were determined by the $2^{-\Delta\Delta CT}$ method. The primer sequences used in this study are shown in Supplementary Tables S1 and S2

Luciferase assay

An ICAM1 or CCL2 promoter-driven luciferase reporter plasmid (firefly) was co-transfected with a Renilla luciferase reporter plasmid into HEK293T cells. A dual-luciferase reporter assay system was used to detect the luminescence, and the activity of NF-κB was shown by the ratio of firefly luminescence to Renilla luminescence.

Chromatin immunoprecipitation (ChIP) assay

Approximately 1×10^6 cells were cross-linked with 1% formaldehyde for 10 min at room temperature followed by quenching with 125 mM glycine. The cells were lysed with a lysis buffer containing 50 mM Tris–HCl (pH 7.5), 150 mM NaCl, 1 mM EDTA, 1% Triton X-100, 0.1% SDS, 0.5 mM PMSF, then the genomic DNAs were sonicated into fragments of ∼100–500 bp. The sonicated cell lysates were cleared and incubated with the indicated antibodies for co-immunoprecipitation. The detailed experimental procedures were performed as previously described (29). The primer sequences used in ChIP-quantatitive PCR analysis are shown in Supplementary Table S3.

Patient samples

Lung specimens from patients with pulmonary tuberculosis and fungal pneumonia were obtained in accordance with research ethics board approval from Xinxiang Medical University. The samples isolated from both lesion areas and corresponding adjacent normal areas were subjected to quantitative PCR analysis or immunohistochemical staining as described above. The detailed clinical information of patients is shown in Supplementary Table S4 and S5.

Statistical analysis

All statistical analyses were performed using GraphPad Prism software. Two-tailed Student's *t*-test was used to compare two groups. One-way analysis of variance (ANOVA) followed by Tukey post-hoc test was used for comparisons greater than or equal to three groups. *P*-value <0.05 was considered statistically significant. All data were obtained in at least three independent experiments and are presented as the mean ± standard deviation (SD).

RESULTS

FOXN3 ameliorates MRSA-induced lung inflammation and injury

An increasing number of studies have shown that the transcription factor FOXN3 is tightly linked to several other regulators of inflammatory response signaling (30–32), although its function in pulmonary inflammatory injury remains unclear. To better understand whether and how FOXN3 contributes to the inflammatory response during lung injury, we first intratracheally instilled LPS into the lungs of mice to induce acute lung injury, then examined the changes in FOXN3 expression. As shown in Supplementary Figure S1A, FOXN3 expression markedly decreased in lungs injured with LPS. To confirm the observed decrease in FOXN3 expression after the occurrence of pulmonary inflammatory injury, we established another *in vivo* model of acute pulmonary inflammation through intratracheal administration of MRSA. We found that FOXN3 expression was also strongly suppressed in the MRSA-infected mice compared with the vehicle (PBS)-treated mice (Supplementary Figure S1B). In line with the *in vivo* observation above, the FOXN3 protein level was dramatically impeded when human ATII or BEAS-2B cells were exposed to the pro-inflammatory stimuli LPS or tumor necrosis factor α (TNFα) *in vitro* (Supplementary Figure S1C, D). These inflammatory injury-responsive changes in FOXN3 expression suggest a likely role in modulating acute lung inflammation and injury.

To define the functional involvement of FOXN3 in acute lung inflammation and injury, *Foxn3* whole-body KO mice were first established using the CRISPR/Cas9 gene editing system (Figure 1A, B) and then subjected to intratracheal administration of MRSA. Although it is difficult to obtain homozygous *Foxn3*-KO mice, the heterozygous *Foxn3*-KO mice exhibited greater neutrophil influx, alveolar edema, wall thickening and permeability relative to WT mice under MRSA infection, as demonstrated by H&E histological staining (Figure 1C). Consistent with this finding, pulmonary inflammatory infiltration of macrophages was also moderately increased after *Foxn3* KO (Figure 1D). Likewise, the mRNA levels of pro-inflammatory factors in the lungs of *Foxn3*-KO mice were elevated compared with that in lungs of WT mice under MRSA infection (Figure 1E). We next extracted BAL fluid and then determined the alveolar permeability. As expected, the total protein concentrations in BAL fluid isolated from *Foxn3*-KO mice showed a moderate increase relative to that from WT mice (Figure 1F). Similarly, the neutrophil-associated MPO activity, WBC counts and levels of the secreted inflammatory cytokines IL-1β and IL-6 in the BAL fluid of *Foxn3*-KO mice were also augmented compared with that of WT mice (Figure 1G–J). To verify the FOXN3-mediated inhibition of pulmonary inflammatory injury, we further constructed an AAV vector to stably overexpress

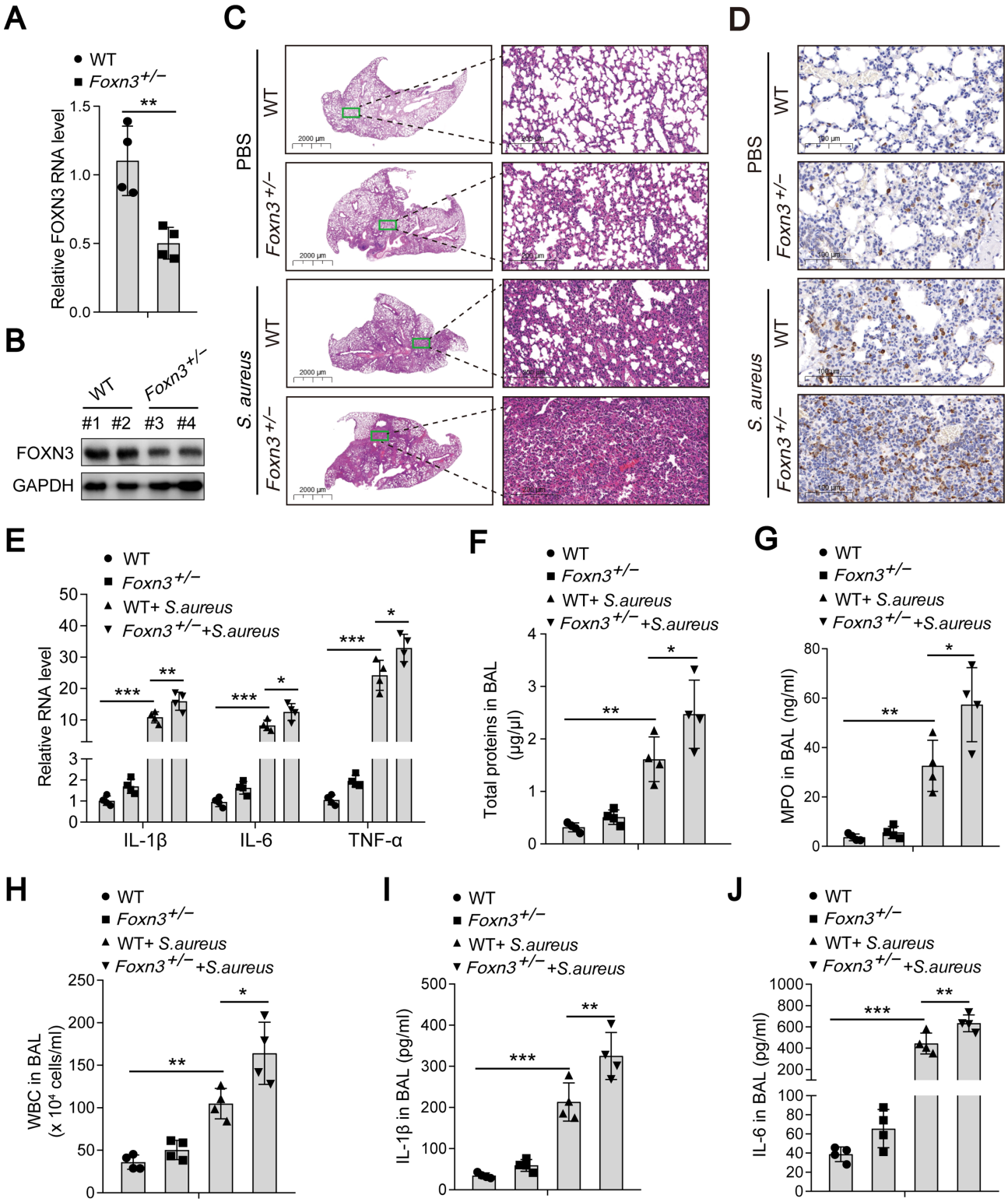

Figure 1. FOXN3 disruption induces pulmonary inflammation and injury. (**A**) Quantitative PCR analysis of FOXN3 RNA levels in lungs of WT or FOXN3-KO mice ($n = 4$). (**B**) Immunoblot analysis of the FOXN3 protein levels in lungs of WT or FOXN3-KO mice. (**C**) H&E histological staining of lung sections from WT or FOXN3-KO mice infected with MRSA or a vehicle (PBS) control. (**D**) Anti-CD68 immunohistochemical staining of lung sections from WT or FOXN3-KO mice infected with MRSA or a vehicle (PBS) control. Scale bars, 100 μm. (**E**) Quantitative PCR analysis of pro-inflammatory factor expression in lungs of WT or FOXN3-KO mice infected with MRSA or a vehicle (PBS) control ($n = 4$). (**F**) BCA analysis of total protein concentrations in BAL fluid from WT or FOXN3-KO mice infected with MRSA or a vehicle (PBS) control ($n = 4$). (**G**) Neutrophil enzyme MPO measurement in BAL fluid from WT or FOXN3-KO mice infected with MRSA or a vehicle (PBS) control ($n = 4$). (**H**) WBC counts in BAL fluid from WT or FOXN3-KO mice infected with MRSA or a vehicle control ($n = 4$). (**I** and **J**) ELISA of IL-1β (I) or IL-6 (J) in BAL fluid from WT or FOXN3-KO mice infected with MRSA or a vehicle (PBS) control ($n = 4$). The data A was assessed by Student's *t*-test and the data E-J were assessed by one-way ANOVA. All data are shown as the mean ± SD. $^{*}P < 0.05$, $^{**}P < 0.01$ and $^{***}P < 0.001$ for comparisons between the indicated groups.

FOXN3 in lung tissues of mice using intratracheal instillation (Supplementary Figure S2A). In line with the findings above, AAV-mediated FOXN3 overexpression significantly impeded MRSA-induced pulmonary inflammatory injury, as determined by the decreased alveolar neutrophil influx, inflammatory infiltration, edema, permeability and the production of pro-inflammatory factors (Supplementary Figure S2B–D), as well as the reduced protein permeability, MPO activity, WBC counts and levels of the inflammatory cytokines IL-1β and IL-6 in the BAL fluid from *Foxn3*-KO mice (Supplementary Figure S2E–I). Collectively, these observations demonstrate that FOXN3 confers strong inhibitory effects on the inflammatory response induced by MRSA-triggered lung injury.

FOXN3 negatively regulates the activation of NF-κB signaling

To elucidate the molecular basis by which FOXN3 affects the inflammatory response during acute lung injury, we performed affinity purification of Flag-tagged FOXN3 coupled with subsequent MS analysis to identify its potential interaction partners. Notably, this analysis identified hnRNPU, a scaffold protein reported to activate NF-κB signaling via control of IκBα stability (20) (Figure 2A, B). An immunoprecipitation assay further confirmed that FOXN3 readily associated with hnRNPU as well as with its known cooperators, including β-TrCP, IKKβ and p38 (Figure 2C; Supplementary Figure S3A). The subcellular fractionation assay revealed that the vast majority of endogenous FOXN3 was localized in the nucleus (Supplementary Figure S3B–D), which aligned well with a previous report showing that the activation of NF-κB mediated by hnRNPU is a nuclear event (20). We therefore hypothesized that FOXN3 might be involved in hnRNPU-mediated NF-κB activation. To test this hypothesis, we first performed immunoblot analysis to determine the effects of FOXN3 on IκBα degradation and found that FOXN3 knockdown led to enhanced ubiquitin-mediated IκBα degradation (Figure 2D, E). In agreement with these results, IκBα stability was obviously increased under FOXN3 overexpression (Figure 2F–H). Moreover, we constructed luciferase reporters driven by either an ICAM1 or CCL2 promoter, both of which are well-known NF-κB transcriptional targets, then examined the effects of FOXN3 overexpression on NF-κB transcriptional regulation of its targets. Interestingly, we found that the transcriptional activation of NF-κB was inhibited under high FOXN3 expression (Supplementary Figure S3E, F). Consistent with this effect, ChIP coupled with quantitative PCR analysis showed that the elevated FOXN3 level led to a crucial blockage of NF-κB recruitment to its target gene promoters and the subsequent transcriptional activation (Figure 2I, J). Taken together, these results further suggest that FOXN3 negatively regulates NF-κB activity by controlling the stability of IκBα.

IκBα cytosolic translocation is essential for NF-κB signaling activation in the inflammatory response and is tightly regulated by FOXN3

A previous study has shown that hnRNPU could activate the nuclear NF-κB signaling by ubiquitin-mediated IκBα/NF-κB complex cytosolic translocation when subjected to UV irradiation (20). We therefore asked whether this NF-κB signaling cascade is able to be activated by pro-inflammatory stimuli. To test this hypothesis, we first performed immunofluorescent staining analysis to observe the nuclear distribution of key members of the NF-κB family and its inhibitor protein IκBα in primary ATII and BEAS-2B cells. As shown in Supplementary Figure S4A, B, a subset of p65, NF-κB1 and RelB, as well as IκBα, appear in the nuclear compartment in the unstimulated state. Next, in order to assess whether the nuclear NF-κB could also be activated by a pro-inflammatory stimulus with LPS or TNFα, we extracted BEAS-2B or HEK293T cells to remove the cytosolic component and then used the extracted nuclei for ubiquitination assay. Interestingly, similar to UV irradiation, both LPS and TNFα treatment markedly induced the nuclear IκBα ubiquitination (Figure 3A, B), and additional treatment with the nuclear export inhibitor LMB promoted the nuclear accumulation of this ubiquitinated IκBα along with p65 (Figure 3A–C), but crucially impeded IκBα degradation (Figure 3D, E) and NF-κB transcriptional activation (Figure 3F, G), indicating that the IκBα/NF-κB complex cytosolic translocation is required for IκBα degradation and NF-κB activation. Additionally, this regulatory pattern for NF-κB signaling activation in the inflammatory response was further verified by immunofluorescent staining assay showing that the IκBα/NF-κB complex was clearly sequestered in the nucleus following LMB treatment (Figure 3H, I). Moreover, the NF-κB signaling activation induced by the pro-inflammatory stimuli LPS or TNFα was critically impeded by the highly expressed FOXN3 (Figure 3J–M). Combined with the above-mentioned findings that FOXN3, a nucleus-restricted regulator, interacts with hnRNPU and undergoes degradation when subjected to pro-inflammatory stimuli, we propose a working model in which FOXN3 becomes unstable in response to pro-inflammatory stimuli, which thus abolish its inhibitory effect on nuclear IκBα ubiquitination and cytosolic proteasomal degradation, thereby activating NF-κB signaling (Figure 3N).

FOXN3 competes with IκBα for binding to hnRNPU to inactivate NF-κB signaling

The significant inhibition of IκBα degradation by FOXN3 prompted us to investigate the underlying molecular mechanism. Since hnRNPU reportedly functions as a bridge protein to connect IκBα with its cognate E3 ligase, β-TrCP, through domain-dependent interactions (20), which is required for β-TrCP-mediated IκBα degradation, we speculated that FOXN3 could potentially compete with IκBα for binding to hnRNPU. To verify this hypothesis, we used a co-immunoprecipitation assay to assess the influence of FOXN3 on interactions between IκBα and hnRNPU or F-box domain-deficient β-TrCP [β-TrCP (ΔF)], which is known to improve its substrate binding (33). Notably, FOXN3 overexpression markedly inhibited the exogenous interactions between hnRNPU or β-TrCP (ΔF) and IκBα (AA), a non-degradable IκBα variant with S32A and S36A residue conversions (Figure 4A), and this inhibitory effect conferred by FOXN3 was further validated by the endogenous co-immunoprecipitation assay (Figure 4B, C). We

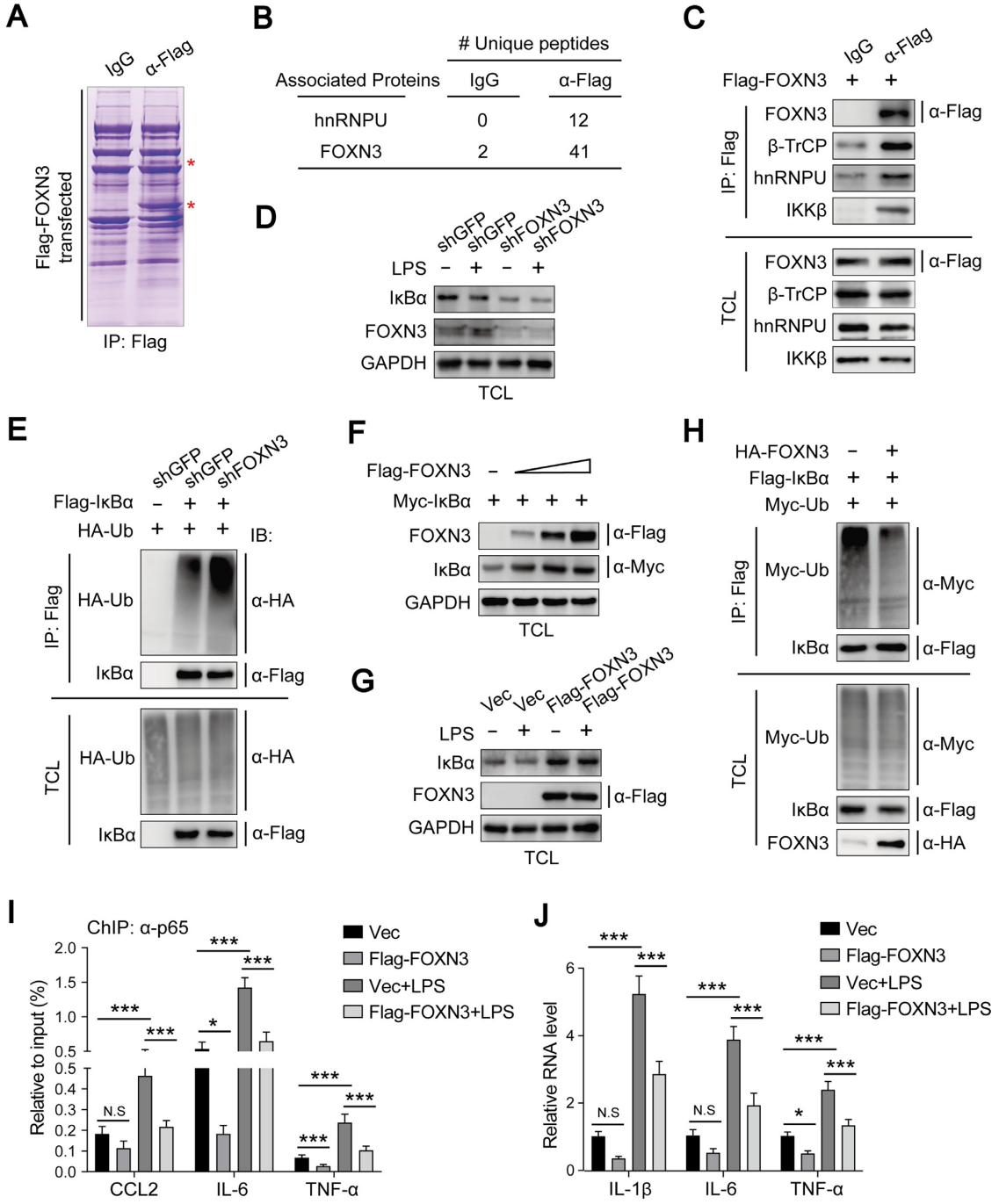

Figure 2. FOXN3 inactivates NF-κB signaling by controlling IκBα stability. (**A**) Coomassie brilliant blue staining of the immunoprecipitates from HEK293T cells. The bands marked with a red asterisk were isolated for subsequent MS analysis. (**B**) MS analysis showing the associated unique peptides from Flag-tagged FOXN3 affinity purification. (**C**) Immunoblot analysis of the endogenous proteins immunoprecipitated by Flag-tagged FOXN3 in BEAS-2B cells as indicated. (**D**) Immunoblot analysis of IκBα expression in total lysates of BEAS-2B cells transduced with lentivirus expressing FOXN3 shRNA or a green fluorescent protein (GFP) shRNA control in the presence or absence of LPS (100 ng/ml, 24 h). (**E**) Immunoblot analysis of IκBα ubiquitination in the lysates of HEK293T cells expressing the indicated combinations of Flag-tagged IκBα, HA-tagged ubiquitin and FOXN3 shRNA. The cells were treated with MG-132 (20 μM, 4 h) before collection. (**F**) Immunoblot analysis of exogenously transfected Myc-tagged IκBα in the lysates of HEK293T cells expressing gradually increasing levels of Flag-tagged FOXN3. (**G**) Immunoblot analysis of IκBα expression in total lysates of human primary ATII cells transduced with lentivirus expressing Flag-tagged FOXN3 or an empty vector control in the presence or absence of LPS (100 ng/ml, 24 h). (**H**) Immunoblot analysis of IκBα ubiquitination in the lysates of HEK293T cells expressing the indicated combinations of Flag-tagged IκBα, HA-tagged FOXN3 and Myc-tagged ubiquitin. The cells were treated with MG-132 (20 μM, 4 h) before collection. (**I**) Anti-p65 ChIP assays showing the NF-κB binding affinity for promoters of its transcriptional targets in BEAS-2B cells transduced with lentivirus overexpressing Flag-tagged FOXN3 or an empty vector control in the presence or absence of LPS (100 ng/ml, 24 h). (**J**) Quantitative PCR analysis of the expression of NF-κB target genes in human primary ATII cells transduced with lentivirus expressing Flag-tagged FOXN3 or an empty vector control in the presence or absence of LPS (100 ng/ml, 24 h). The data I and J were assessed by one-way ANOVA and are shown as the mean ± SD. N.S, not significant; *P <0.05 and ***P <0.001 for comparisons between the indicated groups.

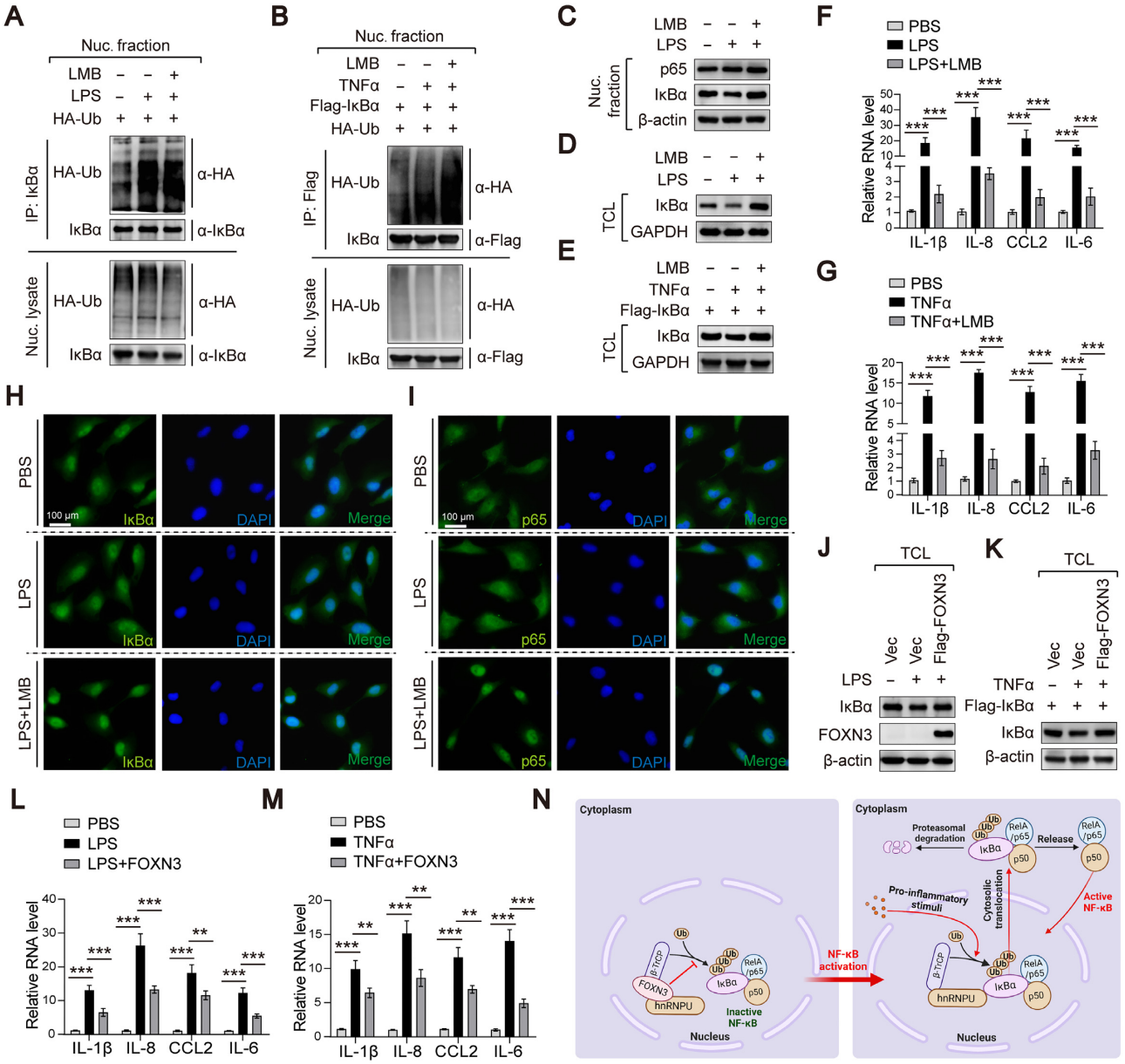

Figure 3. Pro-inflammatory stimuli induce nuclear IκBα ubiquitination and cytosolic translocation for degradation, which is negatively regulated by FOXN3. (**A**) Immunoblot analysis of IκBα ubiquitination in the nuclear lysates of BEAS-2B cells incubated with LPS (20 mg/l) or co-incubated with LMB (15 ng/ml) for 4 h in the presence of MG-132 (20 μM). (**B**) Immunoblot analysis of Flag-tagged IκBα ubiquitination in the nuclear lysates of HEK293T cells incubated with TNFα (20 ng/ml) or co-incubated with LMB (15 ng/ml) for 4 h in the presence of MG-132 (20 μM). (**C**) Immunoblot analysis of IκBα protein levels in nuclear fractions extracted from BEAS-2B cells incubated with LPS (20 mg/l) or co-incubated with LMB (15 ng/ml) for 4 h in the presence of 100 μg/ml CHX. (**D**) Immunoblot analysis of IκBα expression in total lysates of BEAS-2B cells incubated with LPS (20 mg/l) or co-incubated with LMB (15 ng/ml) for 4 h in the presence of 100 μg/ml CHX. (**E**) Immunoblot analysis of the Flag-tagged IκBα expression in total lysates of HEK293T cells incubated with TNFα (20 ng/ml) or co-incubated with LMB (15 ng/ml) for 4 h in the presence of 100 μg/ml CHX. (**F** and **G**) Quantitative PCR analysis of levels of pro-inflammatory factors in BEAS-2B (F) or ATII (G) cells respectively treated with LPS (20 mg/l) and TNFα (20 ng/ml) or co-treated with LMB (15 ng/ml) for 4 h. (**H** and **I**) Immunofluorescent staining analysis showing the subcellular localization of IκBα (H) and p65 (I) in BEAS-2B cells incubated with LPS (20 mg/l) or co-incubated with LMB (15 ng/ml) for 4 h. Scale bars, 100 μm. (**J**) Immunoblot analysis of the endogenous IκBα levels in total lysates of BEAS-2B cells infected with lentivirus overexpressing Flag-tagged FOXN3 or an empty vector control with or without LPS (20 mg/l, 4 h) treatment in the presence of 100 μg/ml CHX. (**K**) Immunoblot analysis of the Flag-tagged IκBα protein levels in total lysates of HEK293T cells overexpressing Flag-tagged FOXN3 or an empty vector control with or without TNFα (20 ng/ml, 4 h) treatment in the presence of 100 μg/ml CHX. (**L** and **M**) Quantitative PCR analysis of levels of pro-inflammatory factors in BEAS-2B (L) and ATII (M) cells infected with lentivirus overexpressing Flag-tagged FOXN3 or an empty vector control in the presence or absence of LPS (20 mg/l, 4 h) or TNFα (20 ng/ml, 4 h). (**N**) A proposed working model depicting the activation of NF-κB signaling regulated by the nuclear FOXN3. The data F, G, L and M were assessed by one-way ANOVA and are shown as the mean ± SD. $^{**}P$ <0.01 and $^{***}P$ <0.001 for comparisons between the indicated groups.

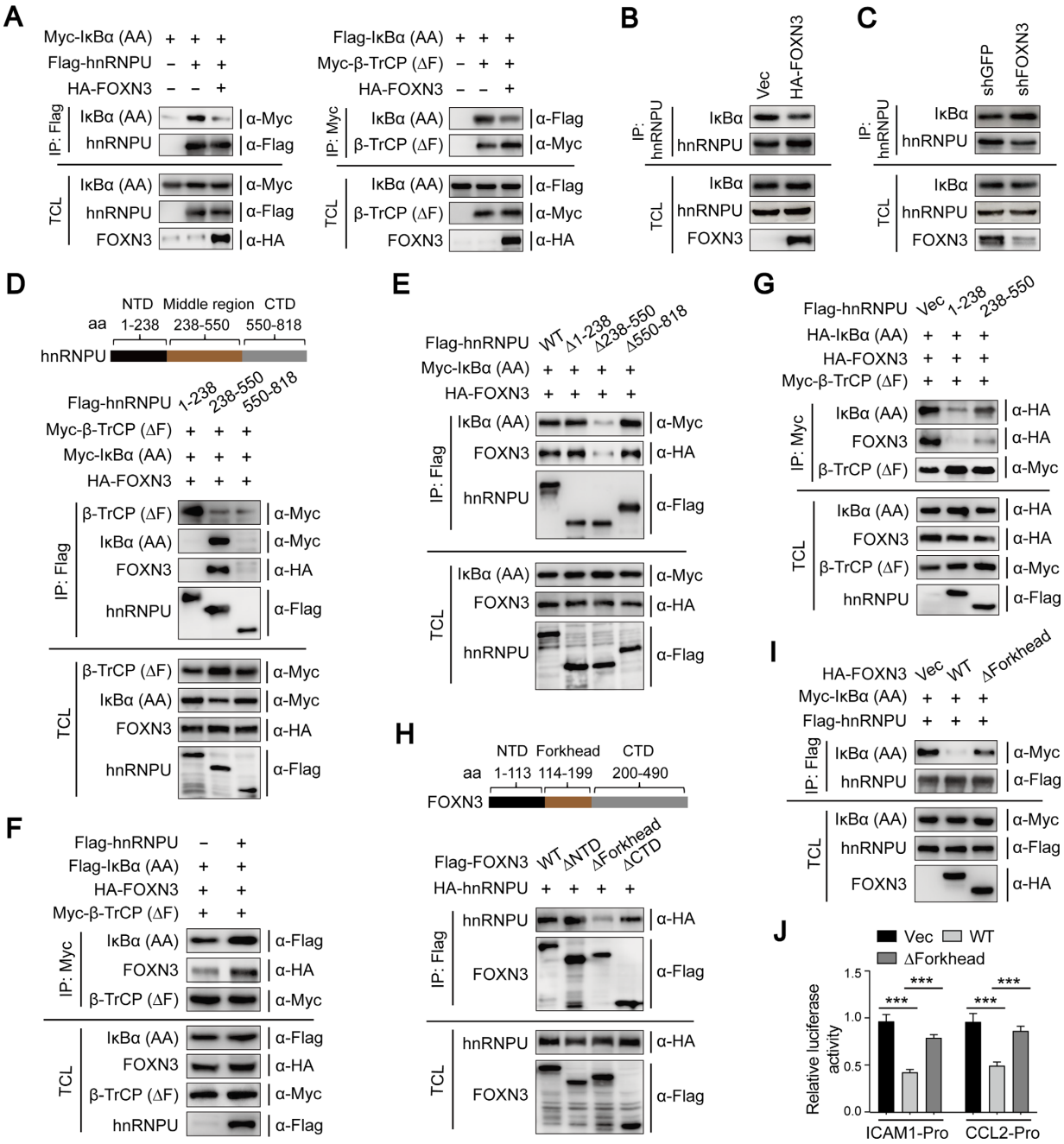

Figure 4. FOXN3 competes with IκBα for binding to the middle region of hnRNPU. (**A**) Immunoblot analysis of Myc-tagged or Flag-tagged IκBα (AA) immunoprecipitated by Flag-tagged hnRNPU (left panel) or Myc-tagged β-TrCP (ΔF) (right panel), respectively, in HEK293T cells with or without HA-tagged FOXN3 overexpression. The cells were treated with MG-132 (20 μM, 2 h) before collection. (**B**) Immunoblot analysis of IκBα immunoprecipitated by endogenous hnRNPU in BEAS-2B cells with or without HA-tagged FOXN3 overexpression. The cells were treated with MG-132 (20 μM, 2 h) before collection. (**C**) Immunoblot analysis of IκBα immunoprecipitated by endogenous hnRNPU in BEAS-2B cells with or without FOXN3 depletion. The cells were treated with MG-132 (20 μM, 2 h) before collection. (**D**) Immunoblot analysis of HA-tagged FOXN3, Myc-tagged β-TrCP (ΔF) and IκBα (AA) immunoprecipitated by Flag-tagged truncated peptides of hnRNPU in HEK293T cells as indicated. The cells were treated with MG-132 (20 μM, 2 h) before collection. (**E**) Immunoblot analysis of HA-tagged FOXN3 and Myc-tagged IκBα (AA) immunoprecipitated by Flag-tagged truncated peptides of hnRNPU in HEK293T cells as indicated. The cells were treated with MG-132 (20 μM, 2 h) before collection. (**F**) Immunoblot analysis of HA-tagged FOXN3 and Flag-tagged IκBα (AA) immunoprecipitated by Myc-tagged β-TrCP (ΔF) in HEK293T cells overexpressing Flag-tagged hnRNPU or an empty vector. The cells were treated with MG-132 (20 μM, 2 h) before collection. (**G**) Immunoblot analysis of HA-tagged FOXN3 and HA-tagged IκBα (AA) immunoprecipitated by Myc-tagged β-TrCP (ΔF) in HEK293T cells overexpressing Flag-tagged hnRNPU deletion mutants or an empty vector as indicated. The cells were treated with MG-132 (20 μM, 2 h) before collection. (**H**) Immunoblot analysis of HA-tagged hnRNPU immunoprecipitated by Flag-tagged truncated peptides of FOXN3 in HEK293T cells as indicated. (**I**) Immunoblot analysis of Myc-tagged IκBα (AA) immunoprecipitated by Flag-tagged hnRNPU in HEK293T cells overexpressing HA-tagged WT or Forkhead domain-deficient FOXN3. The cells were treated with MG-132 (20 μM, 2 h) before collection. (**J**) Luciferase assays showing the inhibitory effect of WT or Forkhead domain-deficient FOXN3 on the transcriptional activity of NF-κB. An ICAM1 or CCL2 promoter-driven luciferase reporter was co-transfected with WT or Forkhead domain-deficient FOXN3 into HEK293T cells. The data J was assessed by one-way ANOVA and is shown as the mean ± SD. ***P <0.001 for comparisons between the indicated groups.

next generated hnRNPU truncation mutants for deletion mapping experiments to define which regions of hnRNPU were required for association with FOXN3. Interestingly, we found that its middle region (amino acids 238–550), also known to be required for IκBα binding, was essential for its interaction with FOXN3 (Figure 4D). Consistent with this, the association between hnRNPU and FOXN3 or IκBα was abolished in the absence of this middle region (Figure 4E), further supporting the fact that FOXN3 competes with IκBα for binding to the middle region of hnRNPU. In line with previous reports, the N-terminal region (amino acids 1–238) of hnRNPU was required for its association with β-TrCP (Figure 4D) and, accordingly, β-TrCP binding with FOXN3 or IκBα was markedly promoted in the presence of hnRNPU (Figure 4F). Moreover, overexpression of either the N-terminal or the middle region of hnRNPU strongly impaired the interaction between β-TrCP and FOXN3 or IκBα by competitive binding (Figure 4G), providing strong support for the notion that hnRNPU functions as a bridge protein that connects β-TrCP with FOXN3 or IκBα via a domain-dependent interaction. Finally, we identified the region within FOXN3 that is essential for its interaction with hnRNPU. The deletion mapping assay showed that deficiency of the FOXN3 Forkhead domain (amino acids 114–199) significantly decreased its association with hnRNPU (Figure 4H). Importantly, lack of the Forkhead domain of FOXN3 failed to prevent the interaction between hnRNPU and IκBα (Figure 4I), and therefore blocked the transcriptional suppression of NF-κB caused by FOXN3 overexpression (Figure 4J). Collectively, these findings suggest that FOXN3, via its Forkhead domain, competes with IκBα for binding to the middle region of hnRNPU, thereby blocking hnRNPU-mediated IκBα degradation and inactivating NF-κB signaling.

P38-mediated FOXN3 phosphorylation promotes its dissociation from hnRNPU

In the FOXN3 affinity purification assay described above, a peptide was trapped in which two consensus residues, S83 and S85, were found to be potential phosphorylation sites in subsequent MS analysis (Figure 5A; Supplementary Figure S5A). To confirm this hypothesis, we converted the two residues, individually and together, from serine to alanine (i.e. S83A, S85A and S83,85A), then quantified the phosphorylation levels of these FOXN3 mutants with an antibody specifically targeting phosphorylated S83 and S85. Both the S85A and S83,85A mutants showed almost total abrogation of FOXN3 phosphorylation, whereas the S83A mutant showed only a moderate decrease in phosphorylation (Figure 5B), suggesting that S85 is the major phosphorylation site of FOXN3.

We next sought to identify the biochemical function of FOXN3 phosphorylation by assaying the effects of FOXN3 phosphorylation on the activation of NF-κB signaling. We found that NF-κB transcriptional activity was further inhibited in the presence of the unphosphorylated S83,85A double mutant compared with that in WT FOXN3, while a phosphomimetic FOXN3 S83,85D mutant led to significant transcriptional induction of NF-κB targets (Figure 5C; Supplementary Figure S5B). As demonstrated above, FOXN3 competitively blocked IκBα recruitment to hnRNPU, thereby inhibiting hnRNPU-mediated NF-κB activation. We therefore asked whether FOXN3 phosphorylation was involved in modulating its interaction with hnRNPU. As predicted, an endogenous co-immunoprecipitation assay revealed that compared with WT FOXN3, the phosphorylation-resistant S83,85A mutant preferentially associated with hnRNPU, thus further preventing IκBα recruitment and binding to hnRNPU (Figure 5D, E). Consistent with this finding, the S83,85A mutation resulted in marked inhibition of ubiquitin-mediated IκBα degradation by β-TrCP compared with WT FOXN3 (Figure 5F; Supplementary Figure S5C), indicating that FOXN3 phosphorylation could potentially induce the activation of NF-κB signaling.

We next sought to identify the upstream kinase that directly phosphorylates FOXN3. Since the p38, casein kinase 2 (CK2) and IKKβ kinases, all of which are hnRNPU cooperators, are functionally involved in hnRNPU-mediated NF-κB activation (20), we thus used a co-immunoprecipitation assay to examine FOXN3 association with hnRNPU, or its partner β-TrCP, in the presence or absence of small-molecule inhibitors specific to each of these kinases. Notably, the p38 inhibitor SB203580, but neither the CK2 inhibitor TBB nor the IKKβ inhibitor IMD-0354, strongly enhanced interactions between FOXN3 and the hnRNPU/β-TrCP complex (Supplementary Figure S5D). Similarly, treatment with SB203580 significantly prevented LPS-induced FOXN3 dissociation from hnRNPU or β-TrCP (Supplementary Figure S5E). More interestingly, a co-immunoprecipitation assay showed that WT FOXN3 dissociated from hnRNPU in the presence of p38, but the S83,85A mutant did not (Figure 5G). In contrast, p38 enhanced the interaction of hnRNPU with IκBα and accelerated β-TrCP-mediated IκBα ubiquitination (Figure 5G, H). Consistent with these results, p38 disruption blocked FOXN3 dissociation from the hnRNPU/β-TrCP complex (Supplementary Figure S5F). To determine whether p38 could directly phosphorylate FOXN3, we first examined the phosphorylation levels of WT FOXN3 and the S83,85A mutant in the presence of p38 and found that the S83,85A double mutant almost completely abolished p38-triggered FOXN3 phosphorylation (Supplementary Figure S5G). Next, we expressed WT FOXN3, the FOXN3 S83,85A mutant and p38 in *Escherichia coli* for purification and subsequent *in vitro* kinase assay. As expected, p38 could directly phosphorylate recombinant WT FOXN3, but not the S83,85A mutant (Figure 5I), demonstrating that FOXN3 is a direct substrate for p38 kinase. Collectively, these results provided strong evidence supporting that p38 directly phosphorylates FOXN3 on its S83 and S85 residues to promote its dissociation from hnRNPU, thus facilitating hnRNPU-mediated IκBα degradation and NF-κB activation (Figure 5J).

p38-mediated FOXN3 phosphorylation accelerates lung inflammation and injury

Given the critical role of FOXN3 phosphorylation by p38 in the activation of NF-κB signaling, we hypothesized that this

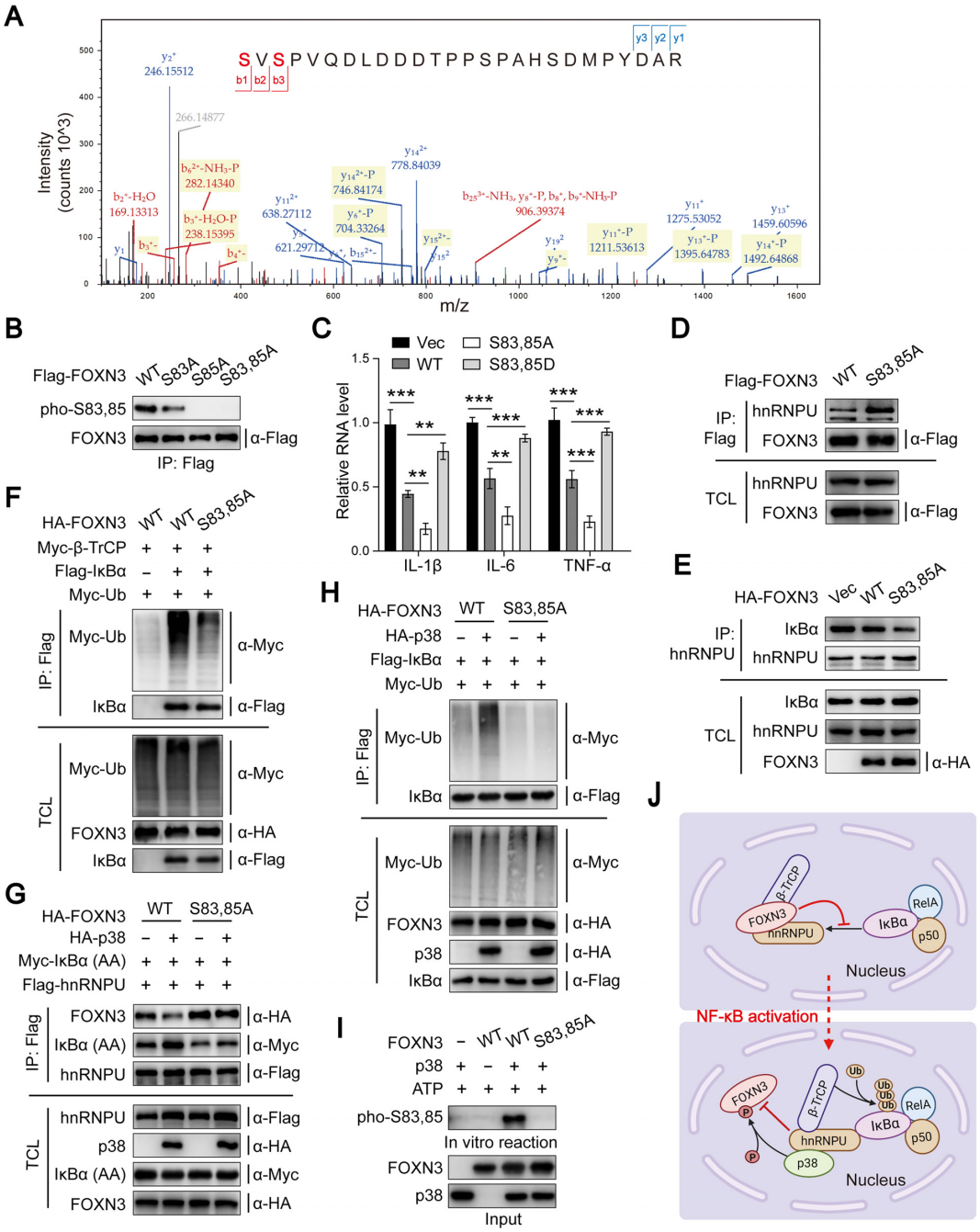

Figure 5. p38-mediated FOXN3 phosphorylation induces its dissociation from hnRNPU and promotes β-TrCP-mediated IκBα degradation. (**A**) FOXN3 phosphorylation at the S83 or S85 residue was identified by tandem MS. The identified peptide is shown. (**B**) Immunoblot analysis of the phosphorylation levels of Flag-tagged WT FOXN3 or its various mutants affinity-purified by anti-Flag immunoprecipitation in HEK293T cells using a phosphospecific antibody targeting either phosphorylated S83 or S85. (**C**) Quantitative PCR analysis of the expression of NF-κB target genes in human primary ATII cells transduced with lentivirus expressing WT FOXN3 or its mutant S83,85A or S83,85D. (**D**) Immunoblot analysis of the endogenous hnRNPU immunoprecipitated by Flag-tagged WT FOXN3 or its S83,85A mutant in BEAS-2B cells. (**E**) Immunoblot analysis of the endogenous IκBα immunoprecipitated by hnRNPU in BEAS-2B cells expressing HA-tagged WT FOXN3 or its S83,85A mutant. The cells were treated with MG-132 (20 μM, 2 h) before collection. (**F**) Immunoblot analysis of IκBα ubiquitination in the lysates of HEK293T cells overexpressing combinations of HA-tagged WT FOXN3 or its S83,85A mutant, Myc-tagged β-TrCP, Flag-tagged IκBα and Myc-tagged ubiquitin as indicated. The cells were treated with MG-132 (20 μM, 4 h) before collection. (**G**) Immunoblot analysis of HA-tagged WT FOXN3 or its S83,85A mutant and Myc-tagged IκBα (AA) immunoprecipitated by Flag-tagged hnRNPU in HEK293T cells with or without HA-tagged p38 overexpression. The cells were treated with MG-132 (20 μM, 2 h) before collection. (**H**) Immunoblot analysis of IκBα ubiquitination in the lysates of HEK293T cells overexpressing combinations of HA-tagged WT FOXN3 or its S83,85A mutant, HA-tagged p38, Flag-tagged IκBα and Myc-tagged ubiquitin as indicated. The cells were treated with MG-132 (20 μM, 4 h) before collection. (**I**) Bacterially expressed p38 and WT FOXN3 or its S83,85A mutant were subjected to an *in vitro* kinase assay, followed by the detection of FOXN3 phosphorylation with a phosphospecific antibody recognizing either phosphorylated S83 or S85. (**J**) A working model for the activation of NF-κB signaling by p38-mediated FOXN3 phosphorylation. The data C was assessed by one-way ANOVA and is shown as the mean ± SD. $^{**}P < 0.01$ and $^{***}P < 0.001$ for comparisons between the indicated groups.

phosphorylation event might be involved in the pulmonary inflammatory response and injury induced by MRSA infection. To determine the functional role of FOXN3 phosphorylation in MRSA-induced acute lung injury, we genetically established a *Foxn3* KI mouse model (*Foxn3*$^{KI/KI}$), in which FOXN3 harbored non-synonymous serine to alanine conversions at both the S83 and S85 sites. As predicted, H&E staining showed that neutrophil influx, alveolar edema and wall thickening were further decreased in *Foxn3* KI mice compared with WT mice after MRSA infection (Figure 6A). We also detected the pulmonary inflammatory infiltration of macrophages and found that *Foxn3* KI mice exhibited decreased pulmonary inflammatory infiltration relative to WT mice (Figure 6B). Accordingly, ablation of FOXN3 S83 and S85 phosphorylation led to significant inhibition of inflammatory cytokine expression in the lungs of mice treated with MRSA (Figure 6C).

To further confirm the regulatory role of FOXN3 phosphorylation in pulmonary inflammation, we collected BAL fluid from MRSA-infected *Foxn3* KI and WT mice to analyze the permeability of lung alveolar cells. Notably, total protein levels in BAL fluid were substantially lower in *Foxn3* KI mice relative to WT mice (Figure 6D). Consistent with this finding, MPO activity, WBC counts and inflammatory cytokine secretion were all dramatically decreased in BAL fluid of the KI mice compared with that from WT mice (Figure 6E–H), indicating that elimination of FOXN3 phosphorylation at the S83 and S85 sites contributes to the improvement of MRSA-triggered pulmonary inflammatory injury. In addition, we further determined whether FOXN3 phosphorylation at S83 and S85 sites is indispensable for p38-promoted pulmonary inflammatory injury. To address this hypothesis, we administrated the p38 inhibitor, SB203580, into both WT and *Foxn3* KI mice to observe whether FOXN3 S83 and S85 phosphorylation is required for p38 deficiency-caused attenuation of pulmonary inflammatory injury. As predicted, histological analysis indicated that the WT mice, but not *the Foxn3* KI mice, showed significant resistance to pulmonary inflammatory injury when subjected to SB203580 administration (Supplementary Figure S6A). In agreement with this, the phosphosite-blocked *Foxn3* KI mice also had no significant effect on pro-inflammatory factor production following SB203580 treatment (Supplementary Figure S6B). Furthermore, the essential role of S83 and S85 phosphorylation in p38-mediated pulmonary inflammation was further validated by BAL fluid assays showing that the BAL fluids from WT mice exhibited an obvious decrease in protein permeability, MPO activity, WBC counts and inflammatory cytokine production after SB203580 administration, whereas the BAL fluids from *Foxn3* KI mice presented no significant changes (Supplementary Figure S6C–G). In summary, these collective findings suggest that FOXN3 S83 and S85 phosphorylation is required for p38-triggered pulmonary inflammatory injury.

FOXN3 dissociated from hnRNPU undergoes phosphorylation-dependent proteasomal degradation

As shown in Supplementary Figure S1, the inflammatory injury-responsive down-regulation of FOXN3 protein indicates that FOXN3 is an unstable protein in response to pro-inflammatory stimuli. To prove this notion, we first treated BEAS-2B cells with LPS in the presence or absence of the proteasome inhibitor MG132 or lysosome inhibitor CQ, then measured the endogenous levels of FOXN3 by immunoblot assay. Consistent with previous findings, LPS induction obviously decreased FOXN3 protein expression (Figure 7A), whereas this down-regulated FOXN3 protein was significantly rescued by MG132 treatment, but not CQ (Figure 7A), suggesting that FOXN3 potentially undergoes proteasome-mediated degradation. According to the data above showing that p38-mediated FOXN3 phosphorylation triggers its dissociation from hnRNPU, we therefore proposed that the phosphorylated FOXN3 that was dissociated from hnRNPU might be unstable and subjected to a proteasome-dependent regulatory mechanism. To test this hypothesis, we first determined the effect of p38 on FOXN3 expression. Intriguingly, p38 overexpression crucially caused the attenuation of FOXN3 protein expression (Figure 7B, C), which was also clearly rescued by MG132 treatment, but not CQ (Figure 7C). Furthermore, inhibition of p38 with shRNA or its inhibitor SB203580 elevated the endogenous protein level of FOXN3 (Figure 7D, E), further confirming that p38 negatively regulates FOXN3 protein expression. Next, we speculated that p38-mediated FOXN3 down-regulation might require S83 and S85 phosphorylation. As predicted, p38 reintroduction significantly blocked the expression of WT FOXN3, but not that of the FOXN3 S83,85A mutant (Figure 7F). Additionally, we isolated the lung tissues of WT mice, as well as those of *Foxn3* KI mice with S83 and S85 double mutations, then measured the changes of FOXN3 protein level. The immunoblot analysis indicated that compared with WT mice, the KI mice exhibited the higher FOXN3 expression level in lung tissues (Figure 7G). In line with this, the MEFs isolated from the *Foxn3* KI mice also showed a clear increase in FOXN3 protein expression relative to those from WT mice, and p38 overexpression triggered the attenuation of the endogenous FOXN3 protein level in WT MEFs, but not that in the MEFs with FOXN3 S83 and S85 double mutations (Figure 7H). To verify the influence of FOXN3 S83 and S85 phosphorylation on its stability, we additionally performed a ubiquitination assay and found that both the inhibitor SB203580 treatment and shRNA-mediated p38 knockdown dramatically prevented FOXN3 polyubiquitination (Figure 7I, J). In agreement with this, the phosphosite-blocked FOXN3 S83,85A mutant was resistant to p38-mediated FOXN3 polyubiquitination (Figure 7K). Collectively, these observations suggest that p38-mediated FOXN3 phosphorylation induces proteasome-dependent FOXN3 degradation.

HnRNPU is required for p38-mediated FOXN3 phosphorylation and phosphorylation-dependent degradation

According to the deletion mapping experiment above showing that the FOXN3 Forkhead DNA-binding domain is essential for its association with hnRNPU, we therefore proposed that FOXN3 recruitment to hnRNPU for the negative regulation of NF-κB signaling might involve a chromatin-dependent mechanism. To prove this hypothesis, we first performed a previously reported fractionation ex-

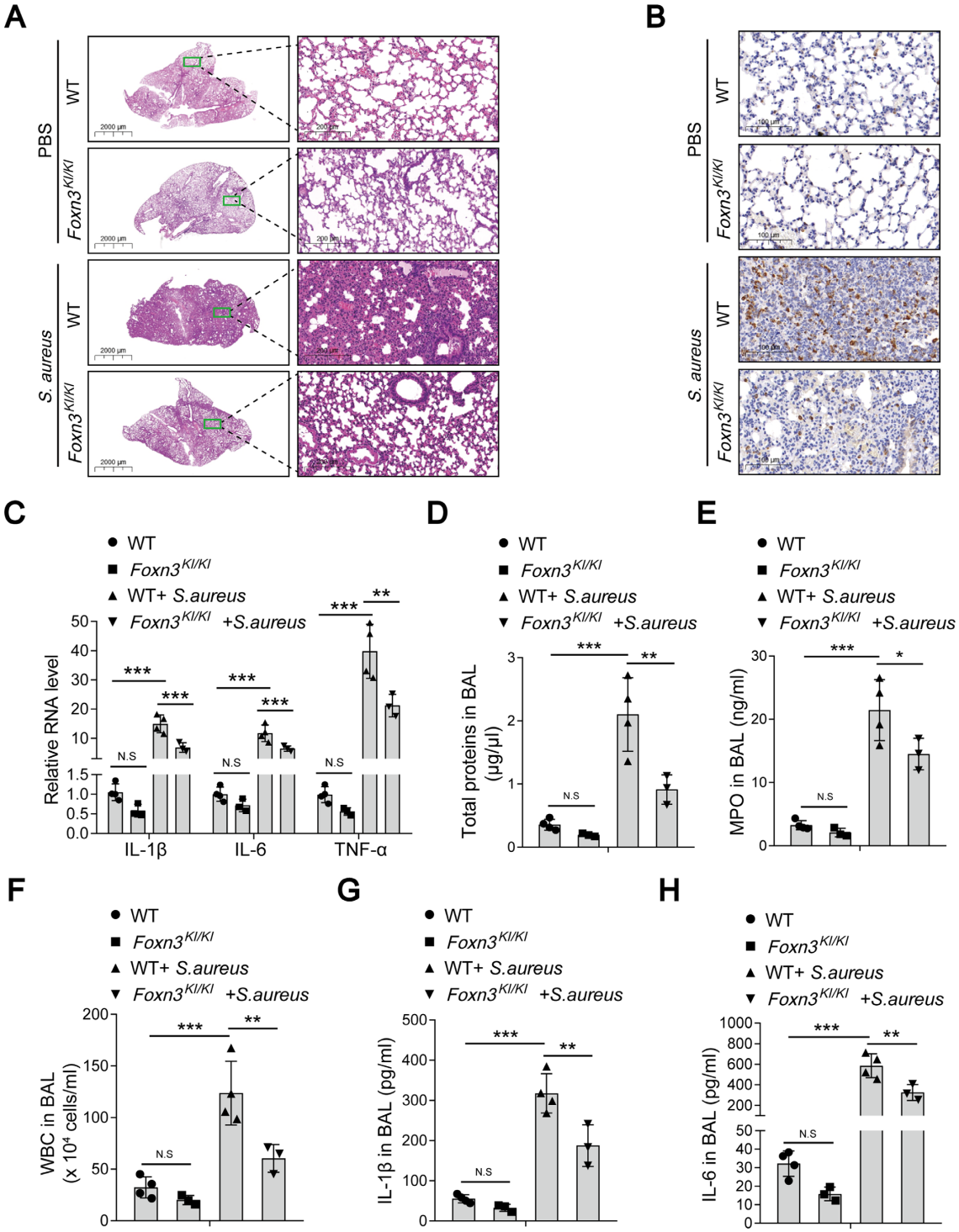

Figure 6. FOXN3 phosphorylation by p38 positively regulates lung inflammation and injury. (**A**) H&E histological staining of lung sections from WT or *Foxn3* KI mice infected with MRSA or the vehicle PBS. (**B**) Anti-CD68 immunohistochemical staining of lung sections from WT or *Foxn3* KI mice infected with MRSA or the vehicle PBS. Scale bars, 100 μm. (**C**) Quantitative PCR analysis of pro-inflammatory factor expression in the lungs of WT or *Foxn3* KI mice infected with MRSA or the vehicle PBS ($n = 4$ for the WT and WT + *S. aureus* groups, $n = 3$ for the $Foxn3^{KI/KI}$ and $Foxn3^{KI/KI}$ + *S. aureus* groups). (**D**) BCA analysis of total protein concentrations in BAL fluid from WT or *Foxn3* KI mice infected with MRSA or the vehicle PBS ($n = 4$ for the WT and WT + *S. aureus* groups, $n = 3$ for the $Foxn3^{KI/KI}$ and $Foxn3^{KI/KI}$ + *S. aureus* groups). (**E**) Neutrophil enzyme MPO measurement in BAL fluid from WT or *Foxn3* KI mice infected with MRSA or the vehicle PBS ($n = 4$ for the WT and WT + *S. aureus* groups, $n = 3$ for the $Foxn3^{KI/KI}$ and $Foxn3^{KI/KI}$ + *S. aureus* groups). (**F**) WBC counts in BAL fluid from WT or *Foxn3* KI mice infected with MRSA or the vehicle PBS ($n = 4$ for the WT and WT + *S. aureus* groups, $n = 3$ for the $Foxn3^{KI/KI}$ and $Foxn3^{KI/KI}$ + *S. aureus* groups). (**G** and **H**) ELISA of IL-1β (G) or IL-6 (H) in BAL fluid from WT or *Foxn3* KI mice infected with MRSA or the vehicle PBS ($n = 4$ for the WT and WT + *S. aureus* groups, $n = 3$ for the $Foxn3^{KI/KI}$ and $Foxn3^{KI/KI}$ + *S. aureus* groups). The data C-H were assessed by one-way ANOVA and are shown as the mean ± SD. N.S, not significant; $^{*}P < 0.05$, $^{**}P < 0.01$ and $^{***}P < 0.001$ for comparisons between the indicated groups.

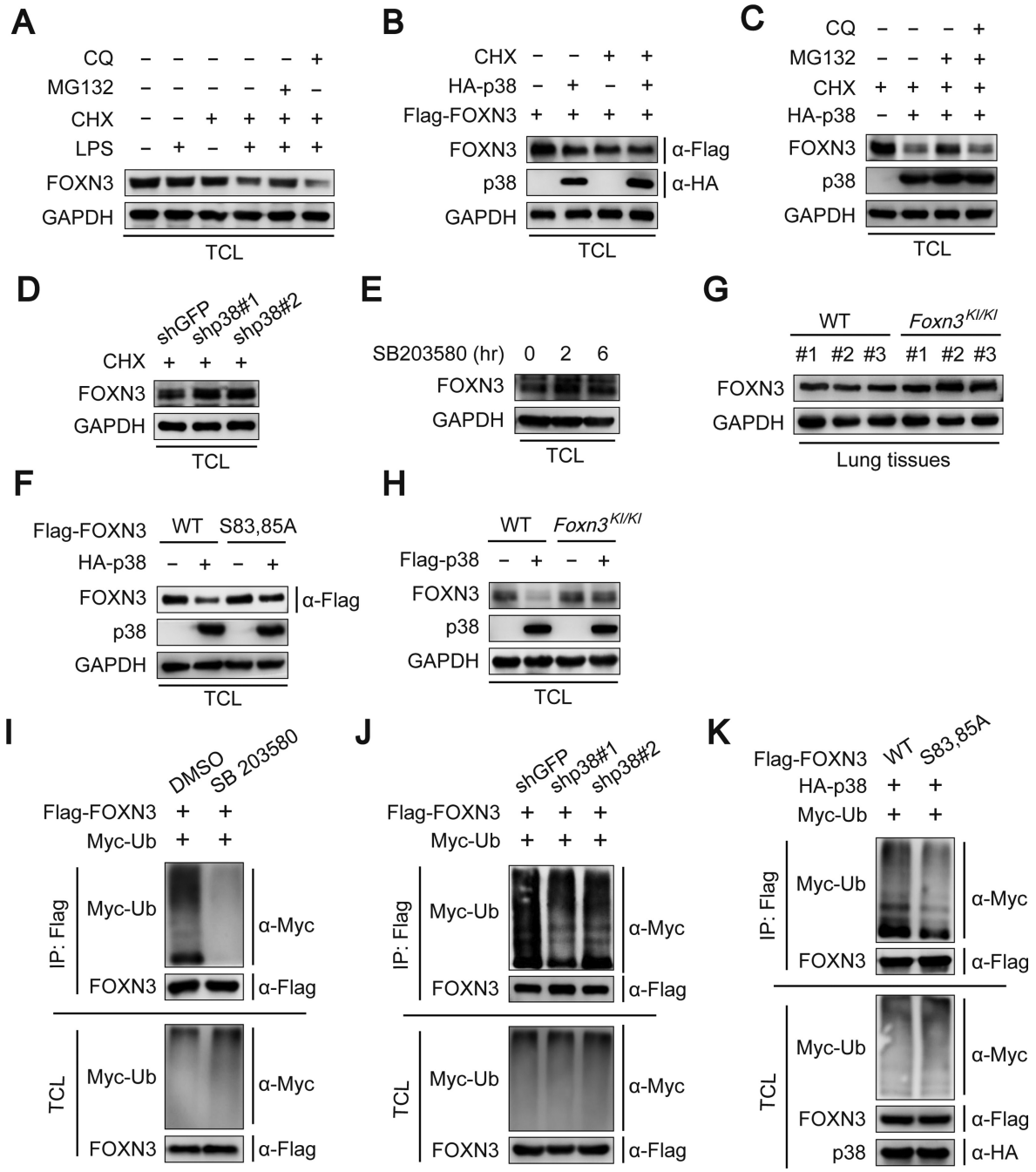

Figure 7. p38 promotes proteasome-dependent degradation of FOXN3. (**A**) Immunoblot analysis of endogenous FOXN3 levels in the total lysates of BEAS-2B cells treated or not with LPS (20 mg/l) or co-treated with MG132 (20 μM) or CQ (25 μM) for 4 h in the presence or absence of CHX (100 μg/ml). (**B**) Immunoblot analysis of Flag-tagged FOXN3 in the total lysates of HEK293T cells with or without HA-tagged p38 overexpression in the presence or absence of CHX (100 μg/ml, 4 h). (**C**) Immunoblot analysis of endogenous FOXN3 protein levels in the total lysates of BEAS-2B cells infected with lentivirus expressing HA-tagged p38 or an empty vector control. The cells were treated with MG132 (20 μM) or CQ (25 μM) for 4 h in the presence of CHX (100 μg/ml) before collection. (**D**) Immunoblot analysis of endogenous FOXN3 protein levels in the total lysates of BEAS-2B cells infected with lentivirus expressing p38 shRNAs or a GFP shRNA control in the presence of CHX (100 μg/ml, 4 h). (**E**) Immunoblot analysis of endogenous FOXN3 protein levels in the total lysates of BEAS-2B cells incubated with SB203580 (20 μM) for the indicated times. The cells were treated with CHX (100 μg/ml, 4 h) before collection. (**F**) Immunoblot analysis of Flag-tagged FOXN3 or its S83,85A mutant in the total lysates of HEK293T cells with or without HA-tagged p38 overexpression. The cells were treated with CHX (100 μg/ml, 4 h) before collection. (**G**) Immunoblot analysis of FOXN3 protein levels in lung lysates from WT or *Foxn3*$^{KI/KI}$ mice. (**H**) Immunoblot analysis of FOXN3 protein levels in the total lysates of MEFs isolated from WT or *Foxn3*$^{KI/KI}$ mice with or without Flag-tagged p38 overexpression. The cells were selected by puromycin (2 μg/ml) for 3 days and then treated with CHX (100 μg/ml, 4 h) before collection. (**I**) Immunoblot analysis of Flag-tagged FOXN3 ubiquitination in the total lysates of HEK293T cells with or without SB203580 (20 μM, 4 h) treatment. The cells were treated with MG132 (20 μM, 4 h) before collection. (**J**) Immunoblot analysis of Flag-tagged FOXN3 ubiquitination in the total lysates of HEK293T cells with or without p38 shRNA knockdown. The cells were treated with MG132 (20 μM, 4 h) before collection. (**K**) Immunoblot analysis of ubiquitination of Flag-tagged WT FOXN3 or its S83,85A mutant in the total lysates of HEK293T cells under p38 overexpression. The cells were treated with MG132 (20 μM, 4 h) before collection.

periment (25) to observe whether the endogenous FOXN3 was associated with chromatin or not (Figure 8A). Surprisingly, we found that FOXN3 was almost completely distributed in the low-salt extracted nuclei (LSEN) specifically consisting of the chromatin-bound proteins (Figure 8B, D). Of note, the chromatin-bound FOXN3 was almost fully released into the supernatant when the LSEN was subjected to DNase I digestion (Figure 8C, E), indicating that the interplay between FOXN3 and hnRNPU occurs in a chromatin-dependent manner.

As a core component, hnRNPU associates with p38, FOXN3, IκBα and multiple regulators engaged in NF-κB signaling modulation via domain-dependent interactions. We therefore hypothesized that hnRNPU might be indispensable for p38-mediated FOXN3 phosphorylation and degradation. As predicted, the FOXN3 affinity purified by immunoprecipitation exhibited an obvious decrease in S83 and S85 phosphorylation after disrupting hnRNPU (Figure 8F), which triggered a marked increase in the total FOXN3 protein level (Figure 8G). In contrast, FOXN3 protein expression was moderately decreased under hnRNPU aberrant overexpression (Figure 8H). Accordingly, the highly expressed hnRNPU led to a slight increase in FOXN3 S83 and S85 phosphorylation (Figure 8I). To characterize whether p38-mediated FOXN3 degradation also relies on hnRNPU, we overexpressed p38 in the presence or absence of hnRNPU. As expected, hnRNPU depletion strongly blocked p38-promoted FOXN3 phosphorylation and phosphorylation-dependent degradation (Figure 8J, K). This observation was in agreement with the ubiquitination assay showing that hnRNPU disruption clearly dampened p38-facilitated FOXN3 ubiquitination (Figure 8L). These findings demonstrate an essential role for hnRNPU in modulating p38-mediated FOXN3 phosphorylation and subsequent phosphorylation-dependent degradation.

FOXN3 phosphorylation is significantly correlated with pulmonary inflammatory diseases

The considerable influence of FOXN3 in determining the development of lung inflammation and injury prompted us to investigate its clinical relevance in pulmonary inflammatory diseases, such as pulmonary tuberculosis and fungal pneumonia. To this end, we performed H&E staining to first verify the inflammatory injury in clinical samples of lung tissues. In agreement with our *in vivo* mouse models, increased inflammatory infiltration, thickened alveolar septa and disruption of alveolar architecture were clearly observed in the lesion samples of the lungs compared with those in the adjacent normal tissues (Figure 9A, B; Supplementary Figure S7A, B). Importantly, we examined the expression levels of total FOXN3, as well as its S83 and S85 phosphorylation, in lungs of these specimens by immunohistochemical staining analysis, and found that consistent with the *in vitro* observation that FOXN3 becomes unstable in response to pro-inflammatory stimuli, the total FOXN3 expression was also clearly decreased in the inflammatory lesion areas compared with that in adjacent normal areas (Figure 9A, B; Supplementary Figure S7A, B). In contrast, the S83 and S85 phosphorylation of FOXN3 which reflects the active status of NF-κB signaling was critically increased when suffering from inflammatory injury during pulmonary infection (Figure 9A, B; Supplementary Figure S7A, B). Similar to these clinical findings, the MRSA infection-induced mice model also presented a marked increase in FOXN3 S83 and S85 phosphorylation compared with the PBS-treated control samples (Figure 9C), although the total level of FOXN3 was decreased after MRSA challenge (Figure 9C). In addition, we further examined the interaction between FOXN3 and hnRNPU in lungs of mice after MRSA infection. As expected, MRSA administration remarkably prevented FOXN3 association with hnRNPU *in vivo* (Figure 9D). In summary, these collective findings provide strong support for the significant positive correlation between FOXN3 phosphorylation and pulmonary inflammatory diseases.

DISCUSSION

MRSA-induced lung injury is an inflammatory pathological process regulated by numerous inflammatory signaling pathways, among which NF-κB signaling is dominant. In this study, we identify the transcription factor FOXN3 as a crucial nuclear regulator which inactivates the nuclear NF-κB signaling, thereby preventing MRSA infection-induced pulmonary inflammatory injury. Our findings show that FOXN3, a nucleus-restricted protein, competes with the NF-κB inhibitory protein, IκBα, for binding to hnRNPU, which results in blockage of hnRNPU-mediated IκBα degradation and inactivation of NF-κB signaling. Although the vast majority of previous investigations have reported that NF-κB family members are primarily distributed in the cytoplasm, sequestered by IκBα in the unstimulated state (14,34–37), a subset of NF-κB family members, as well as their major inhibitory protein IκBα, have been shown to localize in the nucleus of primary ATII and BEAS-2B cells in the absence of stress stimuli, which reflects a nuclear IκBα-involved regulatory mechanism responsible for NF-κB signaling activation. While previous studies have demonstrated that hnRNPU is capable of activating the nuclear NF-κB signaling via ubiquitin-mediated IκBα cytosolic translocation and degradation in response to UV-specific irradiation (20), it remains largely unknown as to whether this regulatory pattern for NF-κB activation could also be utilized under pro-inflammatory stimuli.

Findings in the current work support the obvious induction of nuclear IκBα ubiquitination in response to treatment with pro-inflammatory stimuli, such as LPS or TNFα, and additional treatment with the nuclear export inhibitor, LMB, leads to obvious nuclear accumulation of ubiquitinated IκBα along with NF-κB, consequently leading to strong resistance to pro-inflammatory stimuli-induced NF-κB transcriptional activation, indicating that the nuclear IκBα is targeted for cytosolic translocation and subsequent proteasomal degradation along with NF-κB activation (Figure 9E). This process is similar to the regulatory pattern for UV irradiation-induced NF-κB signaling activation. The functional contribution of the nuclear IκBα ubiquitination to the inflammatory response highlights the essential role of the negative regulator FOXN3 in multiple inflammatory disorders. Overall, both cytosolic and nuclear

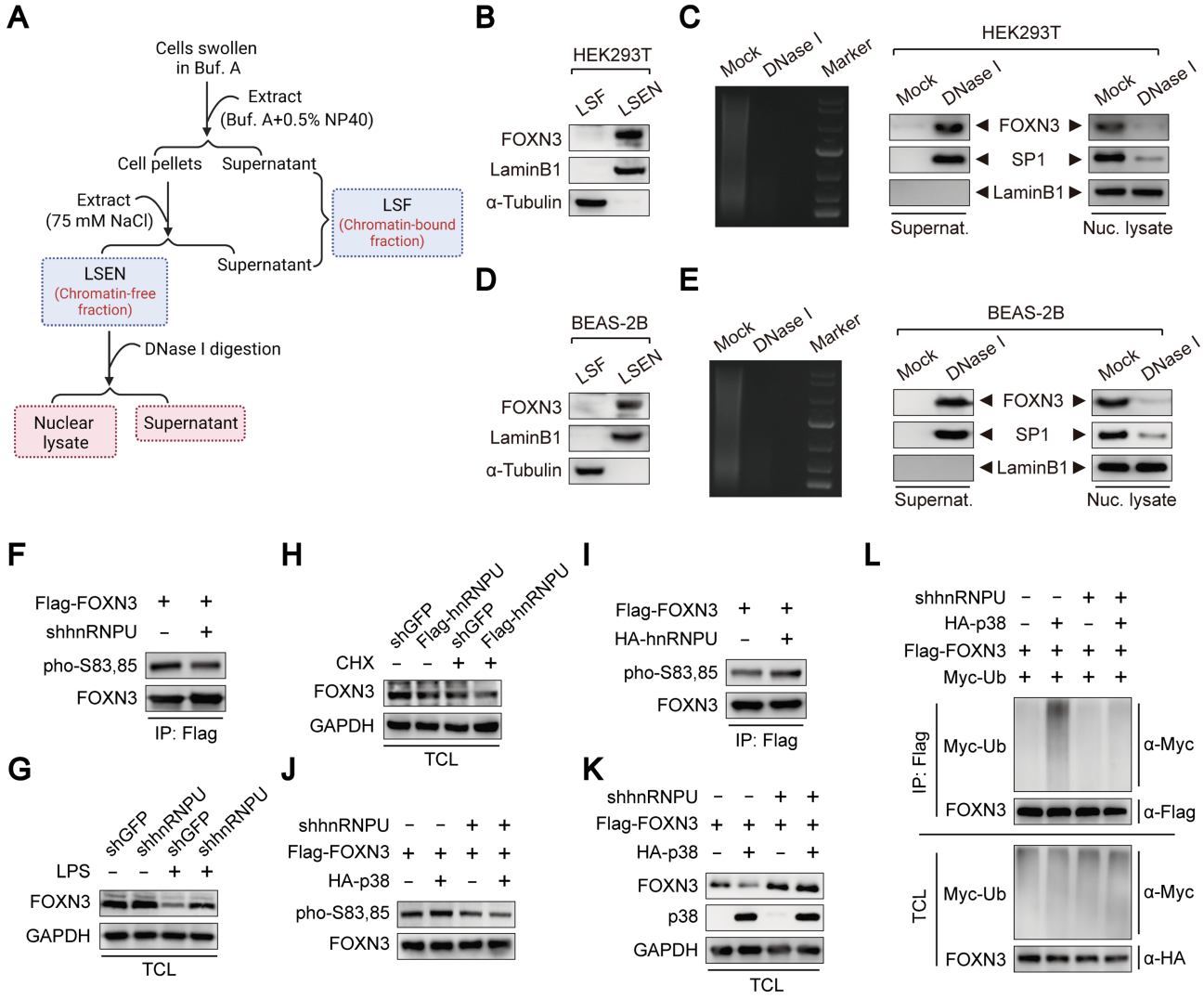

Figure 8. HnRNPU is required for p38-mediated FOXN3 phosphorylation and phosphorylation-dependent degradation. (**A**) A flow chart showing the experimental procedure of nuclear fractionation and DNase I digestion. (**B** and **D**) Immunoblot analysis of chromatin-bound or free FOXN3 extracted from HEK293T (B) or BEAS-2B (D) cells using a fractionation assay. (**C** and **E**) Immunoblot analysis (right panel) of DNase I digestion of the LSEN extracted from HEK293T (C) or BEAS-2B (E) cells. The digestion of chromatin DNA was verified by an ethidium bromide- (EB) stained agarose gel (left panel). The DNA-binding protein SP1 was used as a positive control. (**F**) Immunoblot analysis of S83 and S85 phosphorylation of FOXN3 affinity purified by anti-Flag immunoprecipitation in HEK293T cells with or without hnRNPU knockdown. (**G**) Immunoblot analysis of endogenous FOXN3 levels in BEAS-2B cells transduced with lentivirus expressing hnRNPU shRNA or a GFP shRNA control in the presence or absence of CHX (100 μg/ml, 4 h). (**H**) Immunoblot analysis of endogenous FOXN3 levels in BEAS-2B cells transduced with lentivirus expressing Flag-tagged hnRNPU or an empty vector control in the presence or absence of CHX (100 μg/ml, 4 h). (**I**) Immunoblot analysis of S83 and S85 phosphorylation of FOXN3 affinity purified by anti-Flag immunoprecipitation in HEK293T cells with or without hnRNPU overexpression. (**J**) Immunoblot analysis of S83 and S85 phosphorylation of FOXN3 affinity purified by anti-Flag immunoprecipitation in HEK293T cells after p38 overexpression in the presence or absence of hnRNPU. (**K**) Immunoblot analysis of Flag-tagged FOXN3 levels in HEK293T cells expressing the combinations of Flag-tagged FOXN3, HA-tagged p38 and hnRNPU shRNA as indicated. The cells were treated with CHX (100 μg/ml, 4 h) before collection. (**L**) Immunoblot analysis of Flag-tagged FOXN3 ubiquitination in the total lysates of HEK293T cells expressing the combinations of Flag-tagged FOXN3, HA-tagged p38, Myc-tagged ubiquitin and hnRNPU shRNA as indicated. The cells were treated with MG-132 (20 μM, 4 h) before collection.

regulatory patterns of NF-κB appear to be indispensable for the inflammatory response and may synergistically increase the strength of inflammatory signaling under multiple stimuli. Future work will therefore explore differences in the functional contributions to the inflammatory response between cytosolic and nuclear NF-κB.

As a critical transcription factor, FOXN3 was originally described as a transcriptional repressor involved in the regulation of multiple signaling cascades (31,38–40). Results in this current study show that FOXN3 also serves as an inhibitor of NF-κB signaling, suggesting that FOXN3 is multifunctional and plays diverse biochemical roles in the nuclear compartment through interactions with different regulatory factors. Deletion mapping assays revealed that the FOXN3 Forkhead domain, responsible for its DNA binding capacity, is indispensable for its interaction with hnRNPU and subsequent NF-κB inactivation. This finding demonstrates that FOXN3 recruitment to chromatin

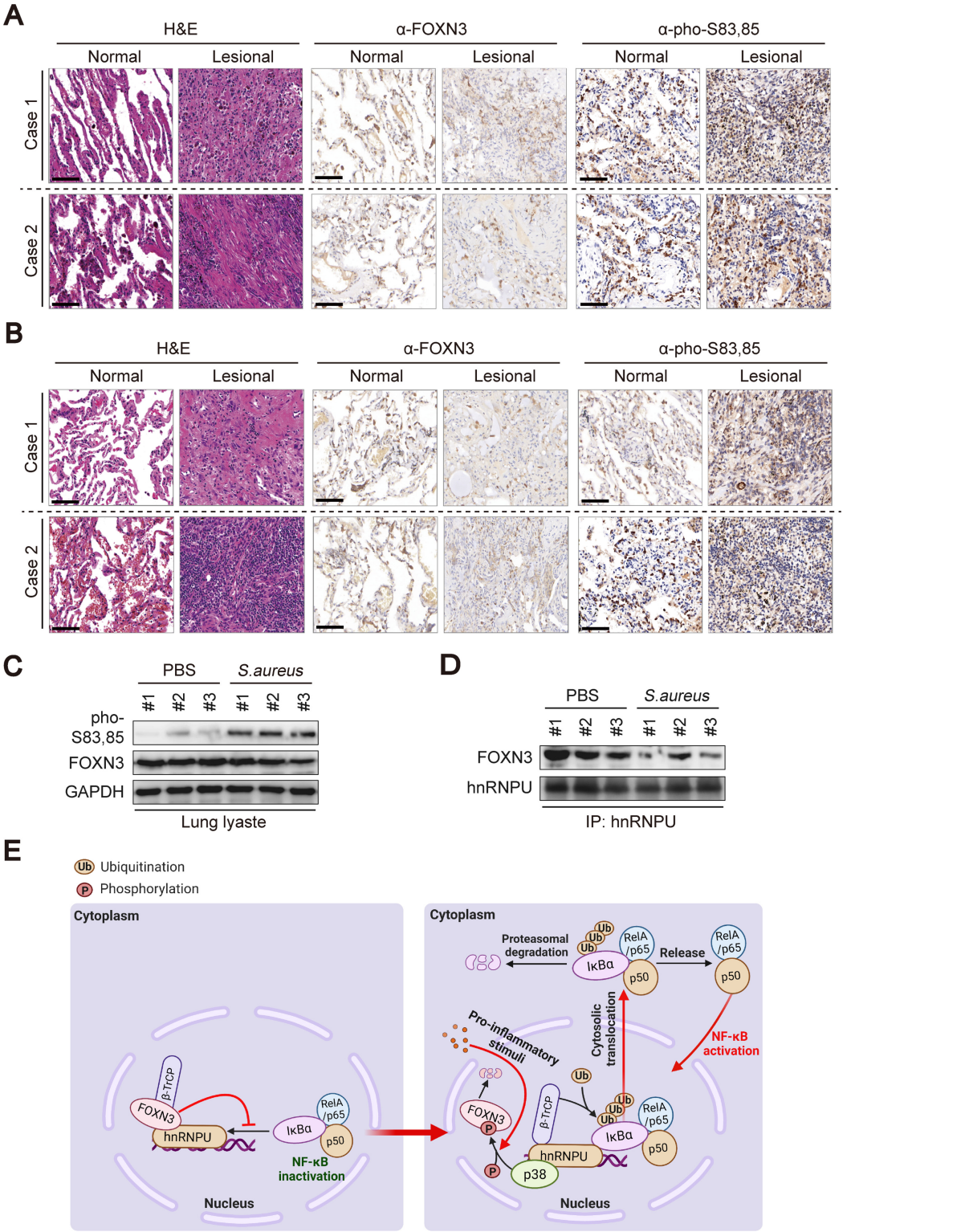

Figure 9. FOXN3 phosphorylation has a significant correlation with pulmonary inflammatory diseases. (**A**) Representative images of anti-total or anti-phosphorylated FOXN3 immunohistochemical staining of lung sections from lesion areas or corresponding adjacent normal areas of seven different patients with pulmonary tuberculosis. H&E staining assay was performed to verify the occurrence of pulmonary inflammatory injury. Scale bars, 100 μm. (**B**) Representative images of anti-total or anti-phosphorylated FOXN3 immunohistochemical staining of lung sections from lesion areas or corresponding adjacent normal areas of six different patients with fungal pneumonia. H&E staining assay was performed to verify the occurrence of pulmonary inflammatory injury. Scale bars, 100 μm. (**C**) Immunoblot analysis of the FOXN3 phosphorylation level in lung lysates of mice infected with MRSA or a vehicle control (PBS). (**D**) Immunoblot analysis of FOXN3 immunoprecipitated by hnRNPU in lung lysates of mice infected with MRSA or a vehicle control (PBS). (**E**) A proposed working model for the activation of NF-κB signaling by p38-mediated FOXN3 phosphorylation in response to pro-inflammatory stimuli.

is required for its inhibition of hnRNPU-mediated NF-κB signaling activation. In agreement with this observation, step-wise fractionation experiments indicated that endogenous FOXN3 is almost completely associated with chromatin, and aligns well with the finding that the FOXN3 released from hnRNPU is unstable and appears to undergo rapid proteasomal degradation. These collective findings provide strong evidence illustrating how FOXN3 utilizes a chromatin-dependent regulatory mechanism to negatively regulate the nuclear NF-κB signaling cascade.

Findings in a previous study suggest that p38, a component of the hnRNPU/IKKβ-integrated complex, can promote hnRNPU-mediated IκBα degradation, resulting in NF-κB activation (20). However, the precise molecular mechanism by which p38 regulates IκBα protein stability has remained poorly understood. In the current study, FOXN3 is shown to serve as a direct substrate for p38 through *in vitro* kinase assay. p38 can directly phosphorylate FOXN3 at its S83 and S85 residues, inducing its dissociation from hnRNPU, consequently promoting IκBα recruitment to hnRNPU for β-TrCP-mediated degradation and therefore activating NF-κB signaling (Figure 9E). In particular, the KI mice with the phosphosite-blocked S83,85A double mutation provide strong evidence that FOXN3 S83 and S85 phosphorylation results in enhanced lung inflammation and injury during MRSA infection. Moreover, WT mice, but not these KI mice, are strongly resistant to pulmonary inflammatory injury triggered by MRSA when subjected to SB203580 administration, further demonstrating that p38-mediated phosphorylation of FOXN3 plays a crucial role in lung inflammation and injury during bacterial infection. To extend our observations to clinicopathologically relevant contexts, we examined clinical lung tissue samples from patients with pulmonary tuberculosis or fungal pneumonia together with adjacent healthy tissue, and found that FOXN3 S83 and S85 phosphorylation was indeed significantly positively correlated with pulmonary inflammation. Hence, targeting FOXN3 could potentially serve as an effective therapeutic strategy for treating pulmonary inflammatory disorders.

HnRNPU, a ubiquitous nuclear scaffold protein functionally involved in modulating chromatin structural organization and chromatin–RNA association, and regulating gene transcription through interactions with various regulatory factors (41–45), was previously found to act as a bridge protein linking β-TrCP with IκBα via domain-dependent interactions. This function of hnRNPU is required for β-TrCP-mediated IκBα degradation and subsequent NF-κB activation (20). Interestingly, our results show that FOXN3 can negatively regulate this process by specifically binding the middle region of hnRNPU essential for IκBα recruitment and ubiquitin-mediated degradation. FOXN3 association with hnRNPU competitively inhibits IκBα recruitment to hnRNPU, thereby blocking IκBα degradation and NF-κB signaling activation. Additionally, hnRNPU is also indispensable for FOXN3 S83 and S85 phosphorylation by recruiting and interacting with p38 kinase. These collective findings clearly illustrate how hnRNPU performs multiple functions to act as a central signaling regulator by establishing a variety of regulatory modules.

DATA AVAILABILITY

The raw data of mass spectrometry have been deposited in the ProteomeXchange Consortium (http://proteomecentral.proteomexchange.org) via the iProX partner repository with the dataset identifier PXD032864.

SUPPLEMENTARY DATA

Supplementary Data are available at NAR Online.

ACKNOWLEDGEMENTS

The schematic diagrams in this study were created with biorender.com.
Author contributions: J. Lin and X.Z. designed and conceived the project. X.Z., B.H. and F.Z. performed most of the experiments. J. Lian and C.M. established the animal models. J.Z. and L.H. collected clinical samples and conducted subsequent analysis. X.Z. and B.H. performed data analysis. X.Z. and J. Lin wrote the manuscript. All authors commented on the manuscript.

FUNDING

This work was supported by grants from National Natural Science Foundation of China [81900392 to X.Z.]; the National Basic Research Program of China [2017YFA0105201 to C.Z.]; the Natural Science Foundation of Henan Province for Distinguished Young Scholars [202300410307 to J. Lin]; and the Deutsche Forschungsgemeinschaft [DFG; YA 721/3–1 and LU 1455/6–1 to X.Y.]. Generation of the FOXN3 mutant mice used in this study was supported by the 111 Program [D20036].
Conflict of interest statement. None declared.

REFERENCES

1. Lowy,F.D. (2003) Antimicrobial resistance: the example of *Staphylococcus aureus*. *J. Clin. Invest.*, **111**, 1265–1273.
2. Choi,Y., He,H., Dodd,M.C. and Lee,Y. (2021) Degradation kinetics of antibiotic resistance gene mecA of methicillin-resistant *Staphylococcus aureus* (MRSA) during water disinfection with chlorine, ozone, and ultraviolet light. *Environ. Sci. Technol.*, **55**, 2541–2552.
3. Peacock,S.J. and Paterson,G.K. (2015) Mechanisms of methicillin resistance in *Staphylococcus aureus*. *Annu. Rev. Biochem.*, **84**, 577–601.
4. Rungelrath,V. and DeLeo,F.R. (2021) *Staphylococcus aureus*, antibiotic resistance, and the interaction with human neutrophils. *Antioxid. Redox Signal.*, **34**, 452–470.
5. Abraham,E. (2003) Neutrophils and acute lung injury. *Crit. Care Med.*, **31**, S195–S199.
6. Lee,W.L. and Downey,G.P. (2001) Neutrophil activation and acute lung injury. *Curr. Opin. Crit. Care*, **7**, 1–7.
7. Mutlu,G.M. and Budinger,G.R. (2006) Incidence and outcomes of acute lung injury. *N. Engl. J. Med.*, **354**, 416–417.
8. Rubenfeld,G.D., Caldwell,E., Peabody,E., Weaver,J., Martin,D.P., Neff,M., Stern,E.J. and Hudson,L.D. (2005) Incidence and outcomes of acute lung injury. *N. Engl. J. Med.*, **353**, 1685–1693.
9. Blank,R. and Napolitano,L.M. (2011) Epidemiology of ARDS and ALI. *Crit. Care Clin.*, **27**, 439–458.
10. Carlson,C.G. and Huang,D.T. (2013) The Adult Respiratory Distress Syndrome Cognitive Outcomes Study: long-term neuropsychological function in survivors of acute lung injury. *Crit. Care*, **17**, 317.

11. Mikkelsen,M.E., Christie,J.D., Lanken,P.N., Biester,R.C., Thompson,B.T., Bellamy,S.L., Localio,A.R., Demissie,E., Hopkins,R.O. and Angus,D.C. (2012) The adult respiratory distress syndrome cognitive outcomes study: long-term neuropsychological function in survivors of acute lung injury. *Am. J. Respir. Crit. Care Med.*, **185**, 1307–1315.
12. Baldwin,A.S. Jr. (1996) The NF-kappa B and I kappa B proteins: new discoveries and insights. *Annu. Rev. Immunol.*, **14**, 649–683.
13. Ghosh,S., May,M.J. and Kopp,E.B. (1998) NF-kappa B and rel proteins: evolutionarily conserved mediators of immune responses. *Annu. Rev. Immunol.*, **16**, 225–260.
14. Hayden,M.S. and Ghosh,S. (2014) Regulation of NF-kappaB by TNF family cytokines. *Semin. Immunol.*, **26**, 253–266.
15. Silke,J. (2011) The regulation of TNF signalling: what a tangled web we weave. *Curr. Opin. Immunol.*, **23**, 620–626.
16. Hayden,M.S. and Ghosh,S. (2008) Shared principles in NF-kappaB signaling. *Cell*, **132**, 344–362.
17. Perkins,N.D. (2007) Integrating cell-signalling pathways with NF-kappaB and IKK function. *Nat. Rev. Mol. Cell Biol.*, **8**, 49–62.
18. Karin,M. and Ben-Neriah,Y. (2000) Phosphorylation meets ubiquitination: the control of NF-κB activity. *Annu. Rev. Immunol.*, **18**, 621–663.
19. Nakayama,K., Hatakeyama,S., Maruyama,S., Kikuchi,A., Onoe,K., Good,R.A. and Nakayama,K.I. (2003) Impaired degradation of inhibitory subunit of NF-kappa B (I kappa B) and beta-catenin as a result of targeted disruption of the beta-TrCP1 gene. *Proc. Natl Acad. Sci. USA*, **100**, 8752–8757.
20. Tsuchiya,Y., Asano,T., Nakayama,K., Kato,T., Karin,M. and Kamata,H. (2010) Nuclear ikkbeta is an adaptor protein for IkappaBalpha ubiquitination and degradation in UV-induced NF-kappaB activation. *Mol. Cell*, **39**, 570–582.
21. Kaestner,K.H., Knochel,W. and Martinez,D.E. (2000) Unified nomenclature for the winged helix/forkhead transcription factors. *Genes Dev.*, **14**, 142–146.
22. Laissue,P. (2019) The forkhead-box family of transcription factors: key molecular players in colorectal cancer pathogenesis. *Mol. Cancer*, **18**, 5.
23. Lehmann,O.J., Sowden,J.C., Carlsson,P., Jordan,T. and Bhattacharya,S.S. (2003) Fox's in development and disease. *Trends Genet.*, **19**, 339–344.
24. Wang,H., Zhou,N., Ding,F., Li,Z., Chen,R., Han,A. and Liu,R. (2011) An efficient approach for site-directed mutagenesis using central overlapping primers. *Anal. Biochem.*, **418**, 304–306.
25. Ai,N., Hu,X., Ding,F., Yu,B., Wang,H., Lu,X., Zhang,K., Li,Y., Han,A., Lin,W. *et al.* (2011) Signal-induced Brd4 release from chromatin is essential for its role transition from chromatin targeting to transcriptional regulation. *Nucleic Acids Res.*, **39**, 9592–9604.
26. Zhu,X., Du,J., Yu,J., Guo,R., Feng,Y., Qiao,L., Xu,Z., Yang,F., Zhong,G., Liu,F. *et al.* (2018) LncRNA NKILA regulates endothelium inflammation by controlling a NF-kappaB/KLF4 positive feedback loop. *J. Mol. Cell Cardiol.*, **126**, 60–69.
27. Voisinne,G., Kersse,K., Chaoui,K., Lu,L., Chaix,J., Zhang,L., Goncalves Menoita,M., Girard,L., Ounoughene,Y., Wang,H. *et al.* (2019) Quantitative interactomics in primary T cells unveils TCR signal diversification extent and dynamics. *Nat. Immunol.*, **20**, 1530–1541.
28. Yuan,W., Lu,L., Rao,M., Huang,Y., Liu,C.E., Liu,S., Zhao,Y., Liu,H., Zhu,J., Chao,T. *et al.* (2021) GFAP hyperpalmitoylation exacerbates astrogliosis and neurodegenerative pathology in PPT1-deficient mice. *Proc. Natl Acad. Sci. USA*, **118**, e2022261118.
29. Zhu,X., Liu,Y., Yu,J., Du,J., Guo,R., Feng,Y., Zhong,G., Jiang,Y. and Lin,J. (2019) LncRNA HOXA-AS2 represses endothelium inflammation by regulating the activity of NF-kappaB signaling. *Atherosclerosis*, **281**, 38–46.
30. Han,T.S., Voon,D.C., Oshima,H., Nakayama,M., Echizen,K., Sakai,E., Yong,Z.W.E., Murakami,K., Yu,L., Minamoto,T. *et al.* (2019) Interleukin 1 up-regulates microRNA 135b to promote inflammation-associated gastric carcinogenesis in mice. *Gastroenterology*, **156**, 1140–1155.
31. Li,W., Zhang,Z., Liu,X., Cheng,X., Zhang,Y., Han,X., Zhang,Y., Liu,S., Yang,J., Xu,B. *et al.* (2017) The FOXN3–NEAT1–SIN3A repressor complex promotes progression of hormonally responsive breast cancer. *J. Clin. Invest.*, **127**, 3421–3440.
32. Wang,C., Tu,H., Yang,L., Ma,C., Hu,J., Luo,J. and Wang,H. (2021) FOXN3 inhibits cell proliferation and invasion via modulating the AKT/MDM2/p53 axis in human glioma. *Aging*, **13**, 21587–21598.
33. Spencer,E., Jiang,J. and Chen,Z.J. (1999) Signal-induced ubiquitination of IkappaBalpha by the F-box protein slimb/beta-TrCP. *Genes Dev.*, **13**, 284–294.
34. Chen,L.F. and Greene,W.C. (2003) Regulation of distinct biological activities of the NF-kappaB transcription factor complex by acetylation. *J. Mol. Med.*, **81**, 549–557.
35. Hoesel,B. and Schmid,J.A. (2013) The complexity of NF-kappaB signaling in inflammation and cancer. *Mol. Cancer*, **12**, 86.
36. Li,Q. and Verma,I.M. (2002) NF-kappaB regulation in the immune system. *Nat. Rev. Immunol.*, **2**, 725–734.
37. Napetschnig,J. and Wu,H. (2013) Molecular basis of NF-kappaB signaling. *Annu. Rev. Biophys.*, **42**, 443–468.
38. Huot,G., Vernier,M., Bourdeau,V., Doucet,L., Saint-Germain,E., Gaumont-Leclerc,M.F., Moro,A. and Ferbeyre,G. (2014) CHES1/FOXN3 regulates cell proliferation by repressing PIM2 and protein biosynthesis. *Mol. Biol. Cell*, **25**, 554–565.
39. Scott,K.L. and Plon,S.E. (2005) CHES1/FOXN3 interacts with ski-interacting protein and acts as a transcriptional repressor. *Gene*, **359**, 119–126.
40. Zhao,C., Mo,L., Li,C., Han,S., Zhao,W. and Liu,L. (2020) FOXN3 suppresses the growth and invasion of papillary thyroid cancer through the inactivation of wnt/beta-catenin pathway. *Mol. Cell. Endocrinol.*, **515**, 110925.
41. Davis,M., Hatzubai,A., Andersen,J.S., Ben-Shushan,E., Fisher,G.Z., Yaron,A., Bauskin,A., Mercurio,F., Mann,M. and Ben-Neriah,Y. (2002) Pseudosubstrate regulation of the SCF(beta-TrCP) ubiquitin ligase by hnRNP-U. *Genes Dev.*, **16**, 439–451.
42. Podgornaya,O.I. (2022) Nuclear organization by satellite DNA, SAF-A/hnRNPU and matrix attachment regions. *Semin. Cell Dev. Biol.*, **128**, 61–68.
43. Xiong,J., Liu,T., Mi,L., Kuang,H., Xiong,X., Chen,Z., Li,S. and Lin,J.D. (2020) hnRNPU/TrkB defines a chromatin accessibility checkpoint for liver injury and nonalcoholic steatohepatitis pathogenesis. *Hepatology*, **71**, 1228–1246.
44. Cao,L., Liu,S., Li,Y., Yang,G., Luo,Y., Li,S., Du,H., Zhao,Y., Wang,D., Chen,J. *et al.* (2019) The nuclear matrix protein SAFA surveils viral RNA and facilitates immunity by activating antiviral enhancers and super-enhancers. *Cell Host Microbe*, **26**, 369–384.
45. Polo,S.E., Blackford,A.N., Chapman,J.R., Baskcomb,L., Gravel,S., Rusch,A., Thomas,A., Blundred,R., Smith,P., Kzhyshkowska,J. *et al.* (2012) Regulation of DNA-end resection by hnRNPU-like proteins promotes DNA double-strand break signaling and repair. *Mol. Cell*, **45**, 505–516.